iScience

Article

Signal transduction pathways controlling *Ins2* gene activity and beta cell state transitions

Graphical abstract

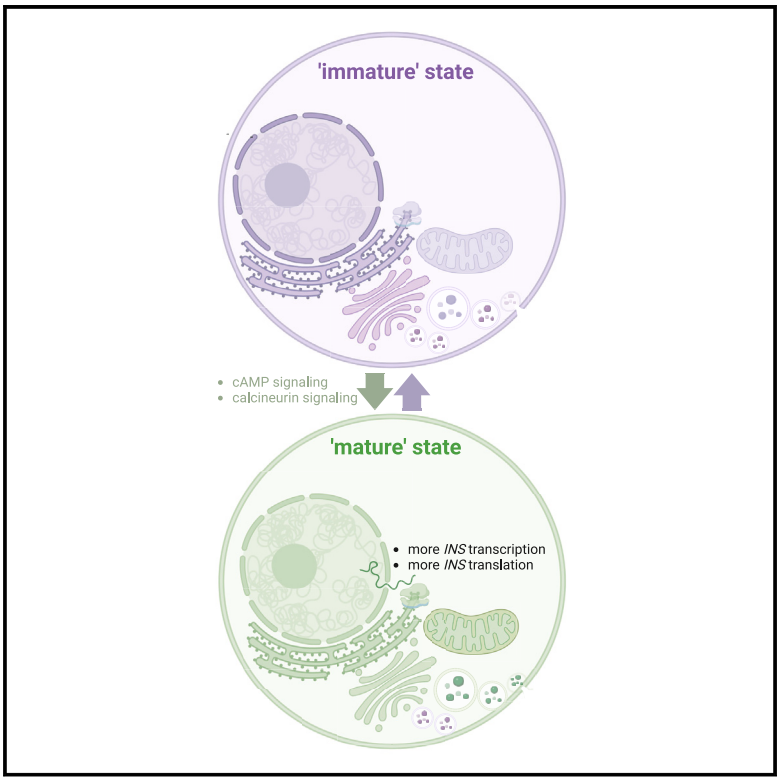

Authors

Chieh Min Chu, Bhavya Sabbineni, Haoning Howard Cen, ..., Yi Han Xia, Jason Rogalski, James D. Johnson

Correspondence

james.d.johnson@ubc.ca

In brief

Biological sciences; Cell biology; Specialized functions of cells

Highlights

- Pancreatic β cells exist in low and high insulin gene activity states that are dynamic
- Cells in the same state were more likely to be nearer to each other in intact islets
- The proteomes of pure β cells show that *Ins2*(GFP)^{HIGH} β cells were more mature
- CAMP signaling activators can drive transitions of *Ins2*(GFP)^{LOW} to the *Ins2*(GFP)^{HIGH} states

Chu et al., 2025, iScience *28*, 112015
March 21, 2025 © 2025 The Authors. Published by Elsevier Inc.
https://doi.org/10.1016/j.isci.2025.112015

CellPress

iScience

CellPress
OPEN ACCESS

Article

Signal transduction pathways controlling *Ins2* gene activity and beta cell state transitions

Chieh Min Chu,[1] Bhavya Sabbineni,[1] Haoning Howard Cen,[1] Xiaoke Hu,[1] WenQing Grace Sun,[1] George P. Brownrigg,[1] Yi Han Xia,[1] Jason Rogalski,[2] and James D. Johnson[1,3,*]

[1]Department of Cellular and Physiological Sciences, Life Sciences Institute, University of British Columbia and the Vancouver Coastal Health Research Institute, Vancouver, British Columbia, Canada

[2]Proteomics and Metabolomics Core Facility, Life Sciences Institute, University of British Columbia, Vancouver, British Columbia, Canada

[3]Lead contact

*Correspondence: james.d.johnson@ubc.ca

https://doi.org/10.1016/j.isci.2025.112015

SUMMARY

Pancreatic β cells exist in low and high insulin gene activity states that are dynamic on a scale of hours to days. Here, we used live 3D imaging, mass spectrometry proteomics, and targeted perturbations of β cell signaling to comprehensively investigate *Ins2*(GFP)^{HIGH} and *Ins2*(GFP)^{LOW} β cell states. We identified the two *Ins2* gene activity states in intact isolated islets and showed that cells in the same state were more likely to be nearer to each other. We report the proteomes of pure β cells to a depth of 5555 proteins and show that β cells with high *Ins2* gene activity had reduced β cell immaturity factors, as well as increased translation. We identified activators of cAMP signaling (GLP1, IBMX) as powerful drivers of *Ins2*(GFP)^{LOW} to *Ins2*(GFP)^{HIGH} transitions. Okadaic acid and cyclosporine A had the opposite effects. This study provides new insight into the proteomic profiles and regulation of β cell states.

INTRODUCTION

Diabetes is characterized by dysfunctional glucose homeostasis which is caused by a relative (type 2 diabetes) or near complete (~80%; type 1 diabetes) deficiency in insulin, the body's main anabolic hormone.[1] Insulin is produced by pancreatic islet β cells, whose dysfunction and/or death are prerequisites for diabetes progression.[2–4] Not all β cells are the same.[5–7] Several studies have shown that insulin content and mRNA can vary greatly between individual β cells.[8,9] Our previous live cell imaging using a dual *Ins1* and *Pdx1* fluorescent promoter reporter showed that mouse and human β cell lines could transition from less to more mature states[10,11] and identified endogenous and chemical regulators of this process.[12,13] However, reporter constructs using abbreviated promoter fragments may not accurately report endogenous gene activity. Therefore, we also used *Ins2*^{GFP} knock-in mice[14] to investigate endogenous *Ins2* gene activity and identified two distinct β cell states, one with high insulin gene activity and higher insulin mRNA, *Ins2*(GFP)^{HIGH}, and one with lower insulin gene activity and lower insulin mRNA, *Ins2*(GFP)^{LOW}.[15] Live cell imaging confirmed that β cells had the capacity to transition between the high and low GFP states in both directions.[15] Single-cell RNA sequencing (scRNAseq) demonstrated *Ins2*(GFP)^{HIGH} cells had a more mature β cell transcriptome profile but were also more fragile.[15] These results suggest that the *Ins2*(GFP)^{HIGH} cells produce more insulin but are also more vulnerable to insults. However, it has been shown that the transcriptome and proteome have weak correlations in islets,[16] so it is critical to understand the proteomic profile of these states. It is also important to understand the molecular mechanisms that control β cell state transitions. ER stress and other cellular perturbations are also known to impact gene transcription.[17,18] For example, stresses associated with the high *Ins2* state lead to β cell fragility[15] and lower proliferation capacity,[19] but the effects of stress itself on *Ins2* gene activity remain unclear. With robotic imaging technology and automated analysis, it is possible to study dozens of signaling pathways at once.

Live imaging of β cell states presented the opportunity for the fluorescence-activated cell sorting (FACS) purification of selected cell populations, while advances in mass spectroscopy permit the identification and cataloging of thousands of cell-selective proteins that could be effects markers or targets for drug delivery. Previous proteomic studies purified β cells using insulin immunofluorescence staining or FAD autofluorescence,[20,21] but these methods for enriching β cells have caveats such as the reliance on antibody specificity and that FAD autofluorescence may not identify all β cells. Thus, there was also a need to revisit those approaches with more sensitive proteomics equipment and analysis pipelines.

Here, we define the proteomic profiles of purified rodent β cells and of the two *Ins2* gene activity states using *Ins2*^{GFP} knock-in mice. We also systematically tested the effects of 48 drugs known to affect selected signaling pathways and cellular functions on *Ins2* gene activity and β cell state transitions. We present a comprehensive comparison of the two *Ins2* expression states at the protein and functional level and reveal multiple genes implicated in mechanisms related to *Ins2* gene activity and β cell state transitions.

This is an open access article under the CC BY-NC-ND license (http://creativecommons.org/licenses/by-nc-nd/4.0/).

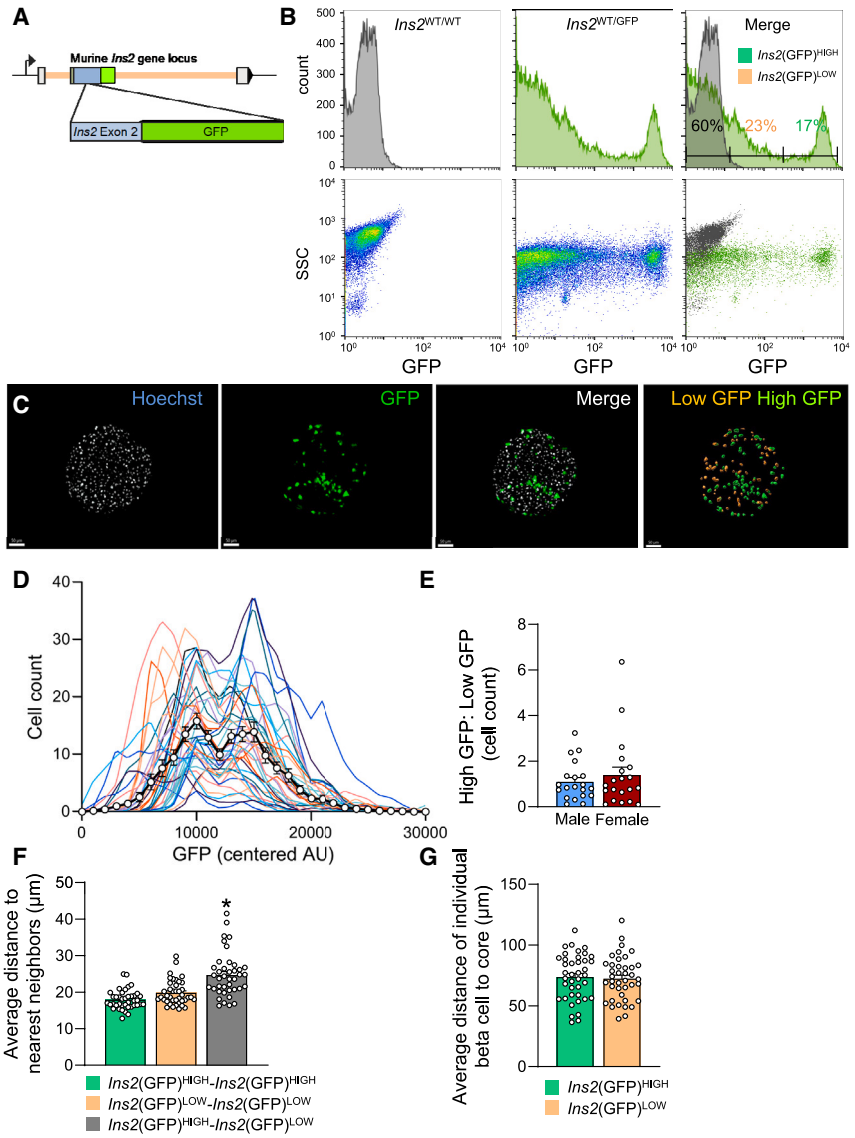

Figure 1. Live 3D imaging of intact *Ins2*^{GFP} mouse islets

(A) Schematic of the *Ins2*^{GFP} knock-in mouse model, in which the second exon of the wildtype *Ins2* gene has been partially replaced with GFP.

(B) FACS purification of *Ins2*(GFP)^{LOW} and *Ins2*(GFP)^{HIGH} populations of β cells, with β cells isolated from a WT mouse for comparison.

(C) Example images of 3D live cell imaging of intact islets from *Ins2*^{GFP} knock-in mice. Hoechst is a cell nuclei dye. Scale bar is 30 μm.

(D) Distribution of cells based on GFP fluorescence from *Ins2*^{GFP} islets. Each distribution line represents an islet. (n = 40 islets).

(E) Comparison of ratios of high GFP cells to low GFP cells in male and female mice. Each dot represents an islet (n = 20 male and 20 female islets from 3 male and 3 female mice).

(F) Nearest neighbor analysis of cells from *Ins2*^{GFP} knock-in mice (n = 40 islets). One-way ANOVA.

(G) Distance to the core of cells from *Ins2*^{GFP} knock-in mice. Student's T-test. Density: probability density function, represents the probability a data is located within the defined range (i.e., ratio of the total). Data are represented as mean ± SEM. *$p < 0.05$.

RESULTS

Live 3D imaging of intact islets from *Ins2*^{GFP} mice

Our previous analyses of *Ins2* gene activity in dispersed mouse islets revealed a bimodal distribution of GFP fluorescence from a reporter construct knocked into the endogenous *Ins2* gene locus[15] (Figures 1A and 1B). In this study, we used live 3D imaging to define the prevalence and spatial relationship of cells in the two β cell insulin gene activity states in whole intact islets from *Ins2*^{GFP} knock-in mice (Figure 1C). We analyzed islets that had below 400 GFP positive cells, as we wanted to avoid large islets that may have necrotic cores.[22] Consistent with dispersed cells, *Ins2* gene activity in intact islets also had a bimodal distribution (Figure 1D). We also found that the range of GFP fluorescence was greater in larger islets compared to smaller ones (Figure 1D). We did not find significant sex differences when comparing the ratios of *Ins2*(GFP)^{HIGH} and *Ins2*(GFP)^{LOW} cells in intact male and female islets (Figure 1E), consistent with our previous work in dispersed β cells.[23] Nearest neighbor analysis showed that cells in the same *Ins2* activity state were more likely to be found in proximity of each other (Figures 1F and S1A). We found no significant difference between the cell states and their distance to the core of the islet (Figures 1G and S1B). To summarize, live cell 3D imaging analysis revealed the that the *Ins2*(GFP)^{HIGH} and *Ins2*(GFP)^{LOW} expression states exist in intact islets, with cells in the same activity states being more likely to be found next to each other.

Identification of β cell selective islet proteins

Proteins that are selective to β cells have potential as biomarkers and anchor targets for imaging and drug delivery.[24] Previous studies have identified β cell-specific mRNAs using single cell RNA sequencing.[25] However, mRNA and proteins in isolated islets only have a correlation coefficient of ~0.5,[16] so there is an unmet need for minimally biased, high-throughput characterization of β cell selective gene products at the protein level. Therefore, as a step toward identifying β cell specific proteins, we compared the proteomes of GFP positive cells to GFP negative cells from dispersed and sorted mouse islets to a depth of 5555 proteins (Figures S2A and S3A). When adjusted for multiple comparisons, 20 proteins were found to be significantly upregulated in GFP negative cells (Figure 2A). These include brain abundant

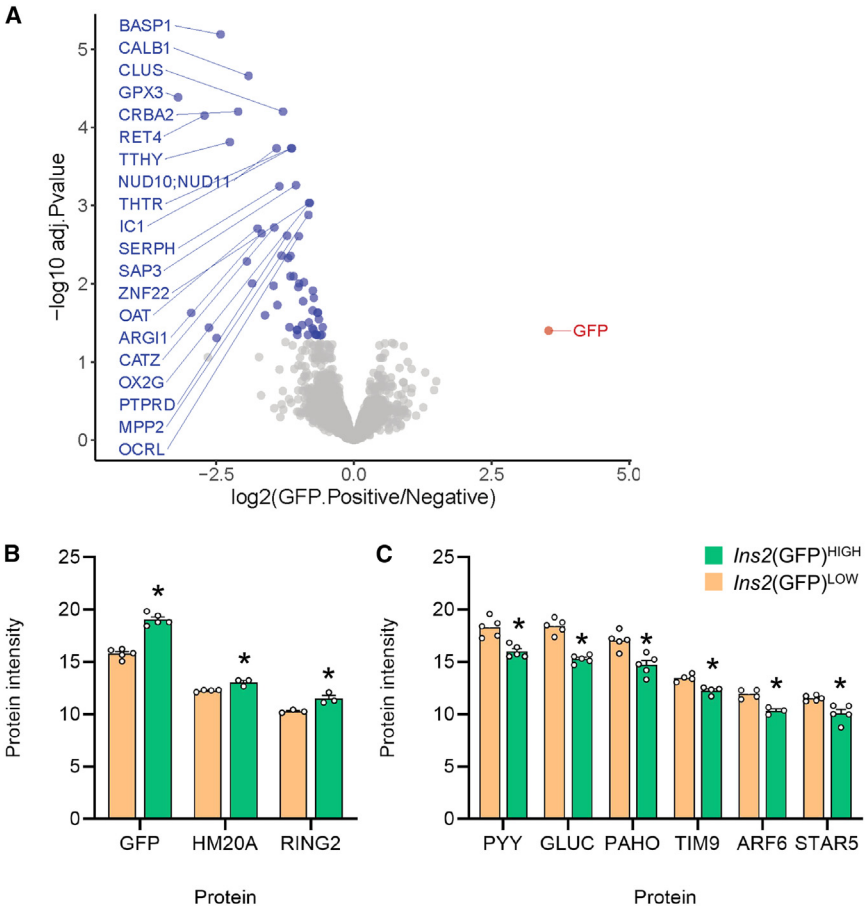

Figure 2. Proteomic analysis of FACS purified *Ins2*^{GFP} β cells

(A) Volcano plot of proteins differentially abundant when comparing GFP positive cells with GFP negative cells.

(B) Barplot of proteins differentially upregulated in *Ins2*(GFP)^{HIGH} cells. *$p < 0.05$.

(C) Barplot of proteins differentially upregulated in *Ins2*(GFP)^{LOW} cells. FACS purified samples were acquired from 3 male and 2 female mice. *$p < 0.05$.

membrane attached signal protein 1 (BASP1), a protein that was found to be upregulated in the islets of non-pregnant mice when compared with pregnant[26]; calbindin 1 (CALB1), a gene that was enriched in δ and γ cells[27]; clusterin (CLU), a protein known to play a regenerative role after islet injury[28]; and glutathione peroxidase 3 (GPX3), a regulator of oxidation that may play a role in T2D associated stress (Figure 2A).[29]

We also undertook a more liberal analysis that did not account for multiple comparisons of our proteomics data. As expected, GFP-negative, non-β cells were enriched for known markers of other islet cell types, such as GCG, PYY, and PPY (Figure S4A). To rank the proteins, we multiplied the *p*-value by the fold change. The top novel non-β cell proteins were the cell surface protein tetraspanin 8 (TSPAN8), arginase 1 (ARG1), and clusterin (CLU) (Figure 2A). The top 5 most significantly enriched β cell selective proteins were: 1) CAP-Gly domain containing linker protein 1 (CLIP1), which links cytoplasmic vesicles to microtubules; 2) 3′-phosphoadenosine 5′-phosphosulfate synthase 2 (PAPSS2), which mediates two steps in the sulfate activation pathway; 3) tyrosine 3-monooxygenase/tryptophan 5-monooxygenase activation protein zeta (YWHAZ), also known as 14-3-3ζ, a scaffolding protein we have shown plays important survival and signaling roles in β cells[30]; 4) apoptosis inducing factor mitochondria associated 1 (AIFM1); and 5) cystathionine beta synthase (CBS), a gene which may play a role in β cell insulin secretion[31] (Figure S4A). As expected, INS1 and IAPP proteins were also significantly enriched in pure β cells. The G protein-coupled receptor 158 (GPR158), a metabotropic glycine receptor[32] which may play a role in autocrine feedback,[33] was highly enriched in β cells.

We next undertook pathway analysis to identify themes in our proteomic data from non-β cells and pure β cells (Figure S4B). Gene set enrichment analyses revealed that non-β cells are enriched for proteins that mediate metabolic and catabolic processes including the "cellular modified amino acid metabolic process" and "carbohydrate derivative metabolic process." In pure β cells, there was enrichment of pathways entitled "skin development" and "supramolecular fiber organization," which was driven by the relative abundance of multiple keratin family proteins, which are known to modulate β cell signaling and play roles in stress responses.[34] Enrichment of the regulation of cellular component biogenesis" and "regulation of protein-containing complex assembly" pathways suggests β cells may exist in a more anabolic state than non-β cells. Pathways involving "protein phosphorylation" and "IκB/NF-κB signaling" were also enriched in pure GFP-positive β cells (Figure S4B). Interestingly, NF-κB signaling has been implicated in a β cell subpopulation with lower PDX1 expression, which has similarities with our *Ins2*(GFP)^{LOW} cells.[35] Overall, these results suggest that differences between *Ins2* expressing cells and other islet cells are primarily associated with protein production and signaling.

Proteomic profiles of fluorescence-activated cell sorting purified β cells in *Ins2*(GFP)^{HIGH} and *Ins2*(GFP)^{LOW} states

We next compared the proteomic profiles of the two distinct *Ins2* gene activity states in FACS purified β cells (Figure S5A). After adjusting for multiple comparisons, we found that, other than GFP, two proteins were significantly upregulated in *Ins2*(GFP)^{HIGH} cells: HMG20A, a protein associated with type 2 diabetes and shown to be important to functional maturity of β cells[36]; and ring finger protein 2 (RING2), a member of the polycomb group of proteins which are important for the

transcriptional repression of genes involved in cell proliferation and development.[37] In the *Ins2*(GFP)^{LOW} state, proteins with greater abundance include the β cell immaturity markers pancreatic polypeptide (PPY), peptide YY (PYY), and glucagon (GCG)[38]; translocase Of inner mitochondrial membrane 9 (TIM9), a protein that helps mediate mitochondrial protein import[39]; ADP ribosylation factor 6 (ARF6), a protein that has been shown to mediate glucose stimulated insulin secretion[40]; and StAR-related lipid transfer domain containing 5 (STARD5), a ER stress protein which helps regulate cholesterol homeostasis.[41] Overall, these findings further support our hypothesis that cells in the *Ins2*(GFP)^{HIGH} state have a more mature β cell profile.

We then analyzed our data without adjusting for multiple comparisons to get an idea of the trends of proteomes of the two cell states. Using *p* value times fold change as a criterion again, the top 5 most enriched proteins in *Ins2*(GFP)^{LOW} cells were: 1) glucagon (GCG), a marker for alpha cells; 2) pancreatic polypeptide (PPY) a marker for PP cells; 3) Purkinje cell protein 4 (PCP4), a calmodulin regulator involved in calcium binding and signaling; 4) aldehyde dehydrogenase 1 family member 3 (ALDH1L2), a mitochondrial enzyme implicated in β cell protection and secretory dysfunction[42]; and 5) adenine phosphoribosyltransferase (APRT), an enzyme involved in the nucleotide salvage pathway (Figure S5A). These results suggest that cells in the less mature *Ins2*(GFP)^{LOW} state was enriched in markers of "multi-hormonal" cells, consistent with our previous scRNAseq analysis.[15] We also found enrichment in proteins in endoplasmic reticulum processing, including HSPA5, HSP90B1, and ERO1L (Figure S8A–S8C), corroborating our prior scRNAseq analyses.[15] The top 5 most enriched proteins (other than GFP) in *Ins2*(GFP)^{HIGH} cells were: 1) zinc finger AN1-type containing 2B (ZFAND2B), a protein associated with the proteasome for the degradation of misfolded proteins; 2) zinc finger RANBP2-type containing 2 (ZRANB2), a protein involved in RNA splicing and mRNA processing 3) myocyte enhancer factor 2D (MEF2D), a calcium regulated transcription factor; 4) SWI/SNF related, matrix associated, actin dependent regulator Of chromatin subfamily A, member 2 (SMARCA2), a protein which regulates transcription via altering chromatin structure; and 5) phosphofurin acidic cluster sorting protein 2 (PACS2), a protein involved in ER calcium ion homeostasis. The protein poly(A) polymerase alpha (PAPOLA), a protein required for the creation of the 3′-poly(A) tail of mRNAs, was also upregulated in *Ins2*(GFP)^{HIGH} cells (Figure S5A).

The pathways significantly enriched in the *Ins2*(GFP)^{LOW} state relative to the *Ins2*(GFP)^{HIGH} state included: "organic acid metabolic process," "cellular respiration," "generation of precursor metabolites and energy," and "oxidative phosphorylation," suggesting the less mature cells may have more energic capacity. They are also enriched in proteins involved in "fatty acid metabolic processes" and "lipid metabolic processes," suggesting the possibility of metabolic substrate preference and switching between these cell states (Figure S5B). The *Ins2*(GFP)^{LOW} state was enriched in the "hormone metabolic process" which was also enriched in non-β cells relative to β cells, including GCG, PYY, and SST. Gene set enrichment analysis revealed that the pathways most enriched in the *Ins2*(GFP)^{HIGH} state were related to transcriptional upregulation and mRNA processing (Figure S5B). The upregulation of "DNA-templated transcription" and "RNA biosynthetic process" pathways may suggest that the *Ins2*(GFP)^{HIGH} state is more transcriptionally active. The *Ins2*(GFP)^{HIGH} state also enriched for "RNA processing," a pathway which involves mRNA capping and addition of the 3′poly(A) tail. Regulation and processing of the 5′ and 3′ UTRs of insulin mRNA is known for their importance in maintaining mRNA stability, and our prior scRNAseq and qPCR data indeed showed that the *Ins2*(GFP)^{HIGH} state had more *Ins2* mRNA.[15] "Chromosome organization" and "cell cycle" pathway upregulation is also indicative of the regulation of the transcriptional landscape. Overall, this data suggests that differences between the *Ins2*(GFP)^{HIGH} and *Ins2*(GFP)^{LOW} states were related to transcription mechanisms and processes.

We next analyzed the relationship between our differentially abundant proteins using STRING and mapped them to a cell diagram in Cytoscape to visualize protein-protein networks in their most common cellular locations (Figures S6A and S6B). Protein-protein interaction networks enriched in GFP negative cells, beyond the known markers from other islet cell types (GCG, PYY, PPY, SST), included protein networks related to lipid metabolism (GPX3, HEXB) and factors related to amino acid synthesis and transport (SLC7A8, SLC3A2, ARG1) (Figure S6A). Protein-protein interaction networks enriched in GFP positive cells, compared with non-GFP, included those involved in GPCR and cAMP signaling, glycolysis, and the secretory pathway (ER, Golgi, granules, cytoskeleton). Specifically, pure β cells showed enrichment for multiple cytoskeletal factors, including VIL1, a member of calcium regulated actin binding proteins and are known to play a role in insulin exocytosis regulation; and CLIP1, a protein associated with granule trafficking.[43–45] These data provide data on β cell specific protein networks at unprecedented detail.

Next, we examined network differences between the *Ins2*(GFP)^{HIGH} state and the *Ins2*(GFP)^{LOW} state. The *Ins2*(GFP)^{LOW} state was enriched for networks related to mitochondria function and cell respiration, including members of the pyrroline-5-carboxylate reductase family (PYCR1, PYCR2), and subunits of the NADH dehydrogenase (ubiquinone) complex (NDUFA6, NDUFB6, NDUFB10) (Figure S7A). We also noted several factors with links to proteasome function (PSMA3, PSMB3, PSMB8), and translation factors (EIF3BEIF4E, EIF4A1) (Figure S7A). This suggests that cells with low *Ins2* gene activity may be recovering from various sources of stress and may also be in the process of regulating translation machinery. Interestingly, RHOA, an F-actin regulator which reduces insulin secretion when activated, was upregulated in the *Ins2*(GFP)^{LOW} state.[46] Another actin protein, ARPC2, which was downregulated in human islets when treated with insulin, was also enriched in *Ins2*(GFP)^{LOW} cells.[47] On the other hand, many of the enriched proteins in the *Ins2*(GFP)^{HIGH} state were located in the nucleus and were linked to transcriptional regulation, including prominent transcription factors TOP1, CDK9, and KAT7(Figure S7B). Several nuclear proteins were associated with mRNA processing, such as ZRANB2, SRPK1, and PAPOLA[48–50] (Figure S7B). We also noted a number of factors in the Golgi, including STRIP1, a protein involved in the localization of the Golgi, and VCPIP1, a protein involved in Golgi reassembly. There were also a fair number of proteins in the ER, including the aforementioned ZFAND2B and PACS2; DNAJA1, a protein that stimulates

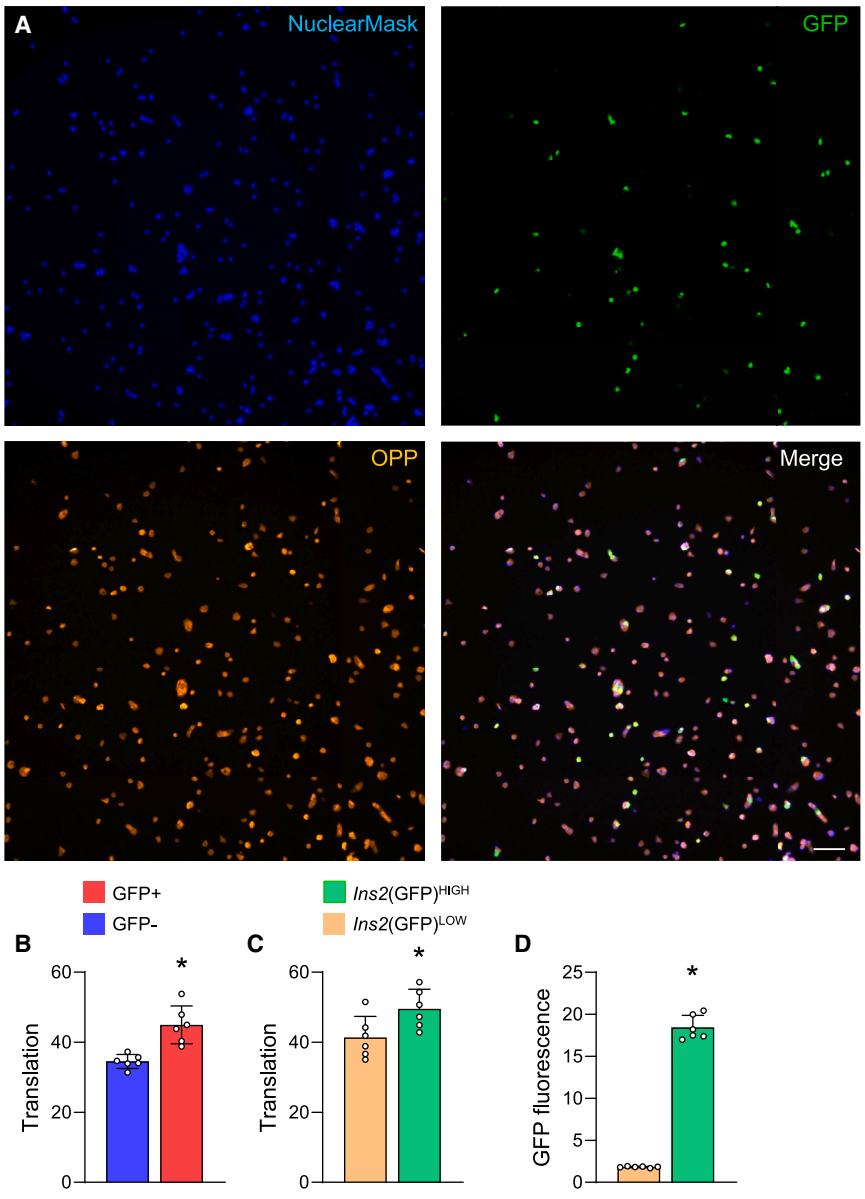

Figure 3. OPP protein synthesis assay of *Ins2*(GFP)^{LOW} and *Ins2*(GFP)^{HIGH} cells

(A) Representative images of OPP protein synthesis assay on *Ins2*$^{WT/GFP}$ mice. The blue wavelength is the Nuclearmask cell nuclei stain, the green wavelength is GFP, and the red wavelength is the OPP marker for nascent peptide formation. Scale bar is 40 μm.

(B) Comparison of translational capacity of GFP positive β cells and GFP negative cells (n = 6 mice, 3 males and 3 females). Student's t test.

(C) Comparison of translational capacity of *Ins2*(GFP)^{HIGH} and *Ins2*(GFP)^{LOW} cells (n = 6 mice, 3 males and 3 females). Student's t test.

(D) GFP fluorescence of *Ins2*(GFP)^{LOW} β cells and *Ins2*(GFP)^{HIGH} β cells. Student's t test (n = 6 mice, 3 males and 3 females). Data are represented as mean ± SEM. *$p < 0.05$.

ATP hydrolysis; and NGLY1, an enzyme involved in the degradation of misfolded proteins. Taken together, the *Ins2*(GFP)^{HIGH} state is primarily associated with the regulation of transcription, mRNA processing, and protein trafficking, while the *Ins2*(GFP)^{LOW} state may be in the process of recovering from stress associated with high *Ins2* gene activity and a shift in protein translation machinery.

Our proteomics data revealed the enrichment of the "regulation of cellular component biogenesis" and "regulation of protein-containing complex assembly" pathways in the *Ins2*(GFP)^{HIGH} state, so we tested whether β cell translation capacity was different compared to other islet cell types using the O-propargyl-puromycin (OPP) assay, which incorporates a fluorescent marker into nascent proteins (Figure 3A). Using GFP as a marker for β cells, we found that β cells had higher translational capacity compared to other islet cells (Figure 3B). The upregulation of DNA template transcriptional regulation and RNA processing pathways in *Ins2*(GFP)^{HIGH} cells relative to *Ins2*(GFP)^{LOW} cells is suggestive of increased downstream translational capacity. We found that cells in the *Ins2*(GFP)^{HIGH} state had significantly higher translational capacity compared to cells in the *Ins2*(GFP)^{LOW} state (Figures 3C and 3D). We did not note any significant differences when comparing the translational capacity of the two *Ins2* expression states in the context of sex differences (Figure S10A). Overall, these data reveal the differences between the *Ins2*(GFP)^{HIGH} and *Ins2*(GFP)^{LOW} expression states at the protein level, and show how some of these differences can translate to differences in β cell function.

Mechanistic interrogation of *Ins2* gene activity regulation

The molecular mechanisms regulating *Ins2* gene activity remain to be fully elucidated. We chose 48 drugs (Table 1) known to perturb key β cell signaling pathways to study their effects on β cell states (Figure 4A). Concentrations for the various compounds were decided based on documented doses used in *in vitro* assays. Dispersed islet cells from *Ins2*^{GFP} mice were treated with compounds and imaged in a high-throughput format (Figures 4B–4L). Although all experiments were conducted in parallel using a robotic imaging system, we visualized the results from each family of compounds separately. Compounds that activate cAMP signaling, namely the PDE inhibitor 3-isobutyl-1-methylxanthine (IBMX) and the cAMP inducer GLP-1, significantly increased *Ins2* gene activity when tracked over time (Figure 4B). The rate of increase for GFP fluorescence was considerably greater in *Ins2*(GFP)^{HIGH} cells in response to cAMP pathway activators compared to *Ins2*(GFP)^{LOW} cells (Figures 5B and 5C). Compared to DMSO control, the calcineurin

Table 1. Reagents used in the small molecule screen

Drug	Concentration	Vendor	Catalog #	Reference
Cyclohexamide	355 μM	Sigma Aldrich	C7698	Hobson et al.[51]
Sal003	5 μM	Sigma Aldrich	S4451	Batista et al.[52]
CCT020312	0.2 μM	Calbiochem	324879	Bruch et al.[53]
DHBDC	20 μM	Calbiochem	5315510001	Bai et al.[54]
ISRIB	0.2 μM	Sigma Aldrich	SML0843	Sekine et al.[55]
GSK2606414/Perk inhibitor 1	0.03 μM	Sigma Aldrich	516535	Axten et al.[56]
PKRi/C16	2 μM	Sigma Aldrich	I9785	Christ et al.[57]
Thapsigargin	1 μM	Millipore	586005	Brownrigg et al.[58]
Tunicamycin	0.1 μM	Sigma Aldrich	T7765	Šereš et al.[59]
Eeyarestatin I	10 μM	Sigma Aldrich	E1286	Wang et al.[60]
APY 29	20 μM	Sigma Aldrich	SML2381	Ghosh et al.[61]
Sunitinib	5 μM	Sigma Aldrich	PZ0012	Lutz et al.[62]
Azoramide	20 μM	Sigma Aldrich	SML1560	Fu et al.[63]
Tacrolimus/FK506	0.03 μM	Selleck Chem	S5003	Oetjen et al.[64]
Cylcosporin A	5 μM	Selleck Chem	S2286	Oetjen et al.[64]
LY 294002	50 μM	Sigma Aldrich	L9908	Beith et al.[65]
Wortmannin	0.1 μM	Sigma Aldrich	W1628	Gao et al.[66]
Sodium butyrate	1000 μM	Sigma Aldrich	B5887	Powers et al.[67]
Trichostatin A (TSA)	0.625 μM	Sigma Aldrich	T1952	Tiernan et al.[68]
MGCD0103/Mocetinostat	25 μM	Selleck Chem	S1122	Fournel et al.[69]
Somatostatin (SST)	1 μM	Sigma Aldrich	S9129	Redmon et al.[70]
Epinephrine	50 μM	Sigma Aldrich	E4250	Redmon et al.[70]
GLP-1 amide	0.01 μM	R&D systems	2082	Skoglund et al.[71]
Rosiglitazone	10 μM	Sigma Aldrich	R2408	Schinner et al.[72]
Staurosporine	0.1 μM	Sigma Aldrich	S4400	Shinozuka et al.[73]
Okadaic	0.1 μM	Sigma Aldrich	O9381	Ammälä et al.[74]
Palmitate	0.5 μM	Sigma Aldrich	P9767	Hagman et al.[75]
Metformin	0.5 μM	Sigma Aldrich	PHR1084	Moon et al.[76]
Dexamethasone (DEX)	0.1 μM	Sigma Aldrich	D4902	Parvin et al.[77]
Isoxazole 9 (ISX-9)	40 μM	Selleck Chem	S7914	Dioum et al.[78]
AS1842856	1 μM	Calbiochem	344355	Zou et al.[79]
Diazoxide	100 μM	Sigma Aldrich	D9035	Ma et al.[80]
IBMX	100 μM	Sigma Aldrich	I5879	Christie et al.[81]
Arginine	10000 μM	Sigma Aldrich	A8094	Leiss et al.[82]
Verapamil	2.7 μM	Sigma Aldrich	V4629	Devis et al.[83]
Ryanodine	10 μM	Millipore	559276	Johnson et al.[84]
5-amino-imidazole carboxamide riboside (AICAR)	300 μM	Sigma Aldrich	A9978	Wang et al.[85]
Pramlintide	1 μM	Sigma Aldrich	SML2523	Suzuki et al.[86]
Tolbutamide	0.37 μM	Sigma Aldrich	T0891	Henquin et al.[87]
HNMPA	100 μM	Abcam	ab141566	Beith et al.[65]
S961	0.1 μM	Phoenix Peptide	051–86	Stamateris et al.[88]
Bortezomib	0.004 μM	Sigma Aldrich	5043140001	Schewe et al.[89]
MG132	0.4 μM	Sigma Aldrich	M8699	Schewe et al.[89]
xestospongin C	2 μM	Sigma Aldrich	X2628	Bito et al.[90]
Actinomycin D	2 μM	Sigma Aldrich	A9415	Bensaude et al.[91]
α-amanitin	2 μM	Sigma Aldrich	A2263	Stellrecht et al.[92]
Triptolide	0.1 μM	Sigma Aldrich	T3652	Stellrecht et al.[92]
5,6-Dichloro-1-beta-Ribo-furanosyl Benzimidazole (DRB)	50 μM	Sigma Aldrich	D1916	Stellrecht et al.[92]

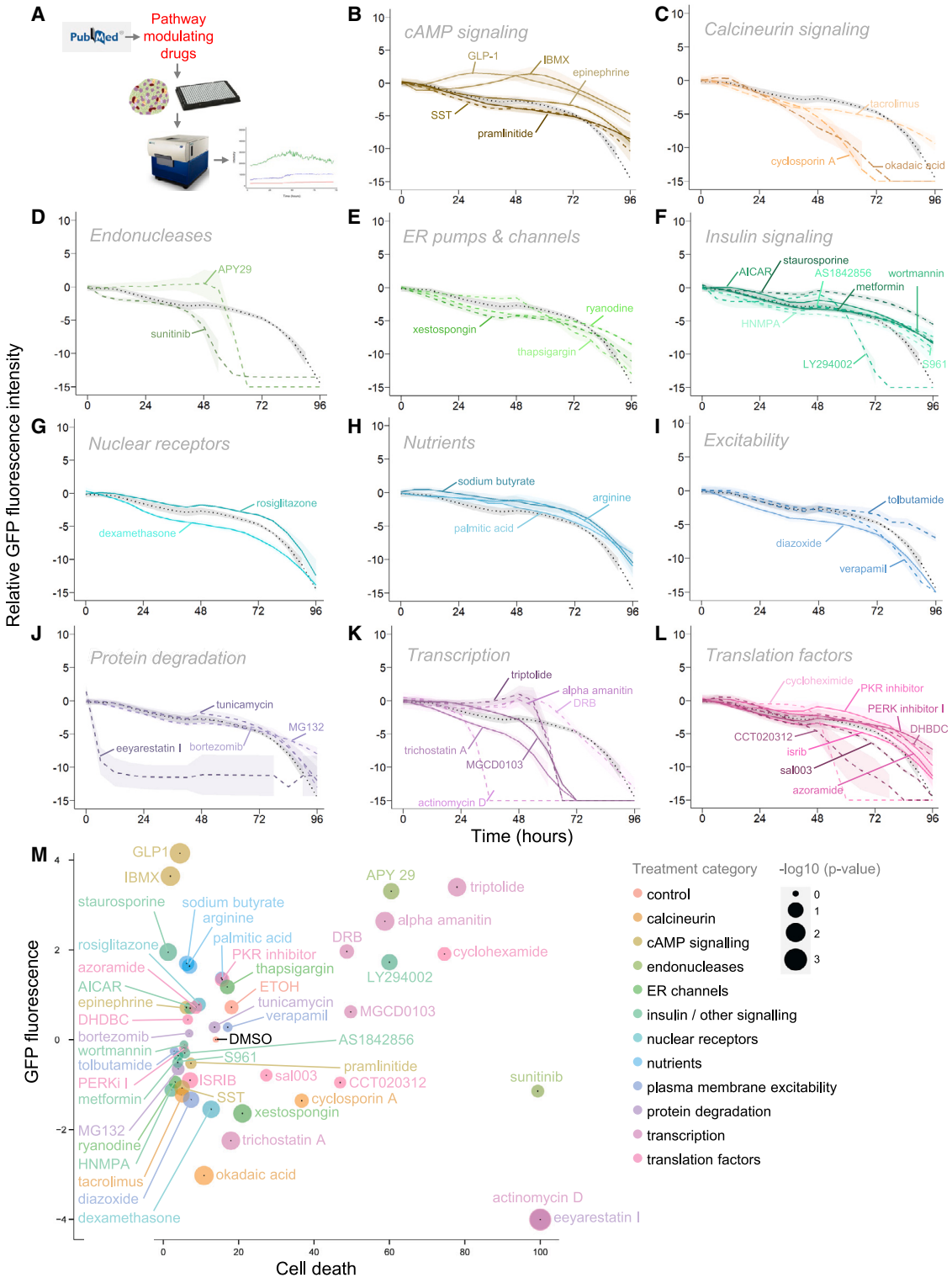

Figure 4. A small molecule screen for effectors of *Ins2* gene activity

(A) Experiment pipeline. Islets were isolated and dispersed from *Ins2*^{GFP} knock-in mice. Cells were then stained with Hoechst cell nuclei dye and propidium iodide (PI) cell death marker for 2 h, and then subjected to treatments. All three fluorescent wavelengths were imaged for 96 h.

(B–L) Average GFP fluorescence of cells over the period of 96 h. Each line represents a treatment. Treatments were categorized based on their primary binding partners. Deceased cells were removed by thresholding for cells with high PI fluorescence. Dotted black lines indicate DMSO controls, dashed lines indicate

(legend continued on next page)

pathway inhibitors cyclosporine A, okadaic acid, and tacrolimus reduced *Ins2* gene activity (Figure 4C). Inhibitors of the endonuclease IRE1A caused a steep drop in *Ins2* gene activity after prolonged treatment, with APY29 inducing a strong increase prior to the drop (Figure 4D). Effectors of ER pumps and channels had relatively few effects on *Ins2* gene activity, with ATP2A2 inhibitor thapsigargin slightly increasing *Ins2* activity (Figure 4E). Compounds that impacted insulin signaling also had some interesting effects, in particular the protein kinase inhibitor staurosporine, which significantly increased *Ins2* gene activity, and PI3K inhibitor LY294002, which caused a spike at 48 h followed by a steep decline (Figure 4F). The glucocorticoid agonist dexamethasone reduced *Ins2* activity, while PPARG agonist rosiglitazone slightly increased it (Figure 4G). The three nutrients we tested all increased *Ins2* gene activity, with arginine and sodium butyrate having a more significant increase over time compared to palmitic acid (Figure 4H). Compounds that affected cell membrane excitability also had interesting effects, with K_{ATP} channel (ABCC8 subunit) activator diazoxide and CACNA1C inhibitor verapamil decreasing *Ins2* gene activity, while K_{ATP} channel (ABCC8 subunit) inhibitor tolbutamide modestly increased it near the end of our experiment (Figure 4I). Perturbing protein degradation factors also yielded effects, in particular ERAD inhibitor eeyarestatin I, which decreased *Ins2* gene activity rapidly after treatment (Figure 4J). As expected, many compounds that affected transcriptional machinery also impacted *Ins2* gene activity (Figure 4K). TFIIH inhibitor Triptolide and RNA polymerase II inhibitor alpha amanitin resulted in an increase in *Ins2* activity, peaking at around 48 h and rapidly declining afterward (Figure 4K). CDK9 inhibitor 5, 6-dichloro-1-β-D-ribofuranosylbenzimidazole (DRB) also increased *Ins2* gene activity (Figure 4K). TOP1 inhibitor actinomycin D caused a steep decline in *Ins2* gene activity 24 h after treatment (Figure 4K). HDAC inhibitors MGCD0103 and trichostatin A both reduced *Ins2* gene activity, but not as abruptly as triptolide and alpha amanitin (Figure 4K). Compounds which affected translation that altered *Ins2* gene activity include EEF2 inhibitor cyclohexamide, which increased *Ins2* activity followed by a steep decline after 48 h, PKR inhibitor, which increased *Ins2* gene activity, and PERK activator CCT020312 and EIF2S1 inhibitor sal003, which reduced *Ins2* gene activity (Figure 4L).

We performed hierarchical clustering using various cell behavior traits in the context of comparing cells from male and female mice. Cell activity traits we used included mean GFP (average GFP fluorescence over time), max GFP (peak GFP fluorescence), and mean cell death (average PI intensity). Overall, the strongest effectors of GFP fluorescence did not show any significant sex differences (Figure S9).

Rapid drops in GFP fluorescence are indicative of cell death, so we explored the relationship between GFP expression and cell viability by plotting fluorescence in the green wavelength (GFP) against the red wavelength (PI) (Figure 4M).[15] We note that the cAMP agonists IBMX and GLP-1 amide had the highest GFP fluorescence with relatively low cell death (Figure 4M). We found that okadaic acid and trichostatin A had the greatest decrease in GFP fluorescence without significant cell death (Figure 4M). The subset of drugs that had increasing GFP fluorescence followed by a rapid drop (APY 29, triptolide, alpha amanitin, cyclohexamide, DRB, LY294002) had significant cell death, indicating the drugs were toxic after prolonged treatment (Figure 4M). This is supported by an OPP assay done in the context of several small molecules of interest (GLP-1 amide, IBMX, APY 29, triptolide), in which a significant drop in translational capacity can be observed after 24 h of treatment, well before the drop in GFP fluorescence and noticeable cell death (Figure S10B). Overall, our small molecule screen shows how various drugs and small molecules may impact *Ins2* gene activity and how it may correlate to β cell health.

Cell state transitions in the context of media conditions and perturbations

Various culture conditions can impact cell state transitions, with higher glucose concentrations and the addition of FBS inducing a greater rate of *Ins2*(GFP)^{LOW} to *Ins2*(GFP)^{HIGH} transitions (Figure 5A). We next analyzed the rate of transitions for cells from *Ins2*^{GFP} knock-in mice in the context of our small molecule screen (Figure 5D). In general, most small molecules had higher *Ins2*(GFP)^{HIGH} to *Ins2*(GFP)^{LOW} transitions rates compared to *Ins2*(GFP)^{LOW} to *Ins2*(GFP)^{HIGH}, with our DMSO control at possessing a ∼3:1 ratio (9.1% *Ins2*(GFP)^{HIGH} to *Ins2*(GFP)^{LOW}, 3.2% *Ins2*(GFP)^{LOW} to *Ins2*(GFP)^{HIGH}). Compared to our DMSO control, we found that cAMP agonists GLP-1 amide and IBMX had the greatest increase in *Ins2*(GFP)^{LOW} to *Ins2*(GFP)^{HIGH} transitions (19% for GLP-1 amide, 14% for IBMX), with relatively low levels of *Ins2*(GFP)^{HIGH} to *Ins2*(GFP)^{LOW} transitions (Figures 5B–5D). Okadaic acid and cyclosporin A induced the highest rate of *Ins2*(GFP)^{HIGH} to *Ins2*(GFP)^{LOW} transitions (Figure 5D). Interestingly, we found that several drugs with high GFP, including triptolide, APY 29, and alpha amanitin, had very few transitions of either type (Figure 5D). This shows that the increase in GFP fluorescence observed in these treatments was primarily driven by increasing GFP fluorescence in the *Ins2*(GFP)^{HIGH} cells, and not in the *Ins2*(GFP)^{LOW} cells.

STRING/Cytoscape analyses helped contextualize the major binding partners of our small molecule screen (Figures 6A and 6B). Several of the strongest effectors of GFP fluorescence were found to impact genes located within the nucleus, including CDK9, TOP1, POL2A, ERCC3, HDAC1, HDAC2, SP1, and PAK1. Many of these proteins have known roles in transcriptional mechanisms.[93–98] On the membrane, GLP1R and NOS1 were receptors that had effects on GFP fluorescence. In the ER, perturbing ERN1, a major factor in UPR response, impacted GFP fluorescence and cell health.[99] In the cytosol, the perturbation of VCP, a major component of ERAD, resulted in heavy cell death,

inhibitors of their respective categories, and solid lines indicate activators of their respective categories (n = 6 mice, 3 males and 3 females). Shading represents SEM.

(M) Analysis of GFP fluorescence against cell death. GFP fluorescence is scaled GFP fluorescence relative to background after 48 h of treatment. Cell death is scaled PI fluorescence relative to background after 72 h of treatment. Size of dots represents p value (adjusted). Colors of dots represents categories, which were decided based on their primary binding partners (n = 6 mice, 3 males and 3 females). two-way ANOVA, adjusted p value indicated by size of dots.

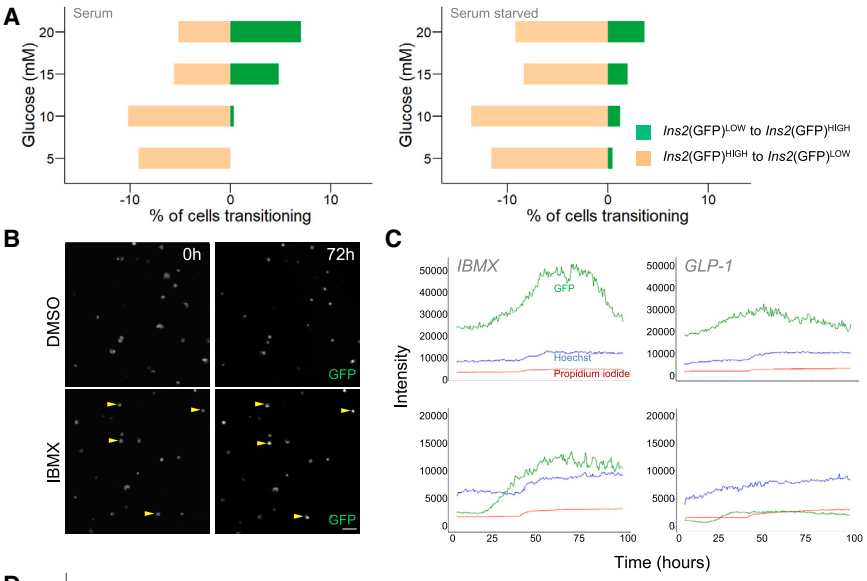

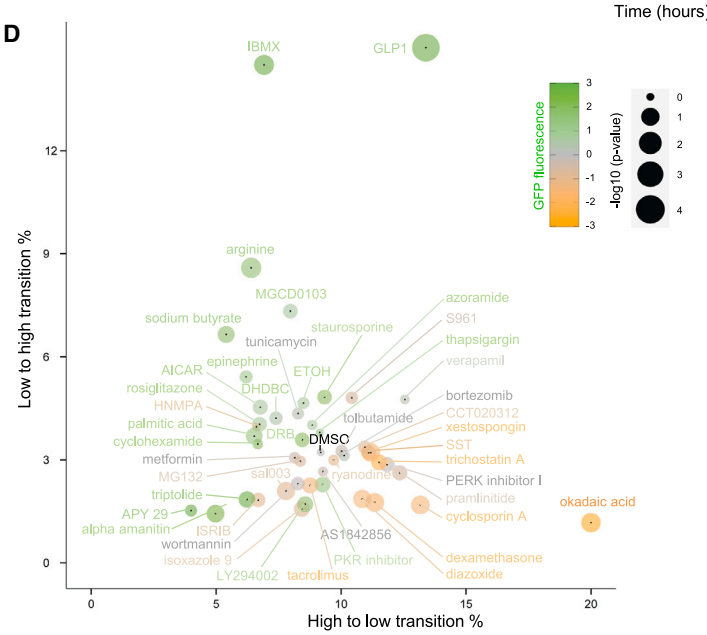

Figure 5. Cell state transitions in the context of various media conditions and perturbations

(A) Transition rates between the *Ins2*(GFP)^{HIGH} and *Ins2*(GFP)^{LOW} cell states in the context of various media conditions. % of cells transitioning: percent of subpopulation transitioning to other cell state after 48 h of culture.

(B) Example images of increasing GFP fluorescence in response to IBMX. Scale bar is 50 μM.

(C) Example traces of GFP upregulation and cell state transitions in response to IBMX and GLP-1 amide.

(D) Comparison of *Ins2*(GFP)^{HIGH} to *Ins2*(GFP)^{LOW} and *Ins2*(GFP)^{LOW} to *Ins2*(GFP)^{HIGH} transition rates in the context of the small molecule screen. Data shown is the average transition rate by the end of 48 h of treatment (n = 6 mice, 3 males and 3 females). Size of the dots denotes p value (adjusted). Color of the dots denotes scaled GFP fluorescence. two-way ANOVA.

while PIK3CA, PDE3A, EEF2 influenced GFP fluorescence. In the context of cell state transitions, perturbing PDE3A and GLP1R induced the highest rate of *Ins2*(GFP)^{LOW} to *Ins2*(GFP)^{HIGH} transitions, while perturbing PPP3CC and PPP2CA resulted in the highest rate of *Ins2*(GFP)^{HIGH} to *Ins2*(GFP)^{LOW} transitions. Overall, these results show how perturbing various β cell signaling pathways may impact *Ins2* gene activity and cell state transitions.

DISCUSSION

This study aimed to further our understanding of dynamic *Ins2* gene activity states, their proteomic profiles, and their regulation by key cellular processes. Several prior studies have labeled β cells using *Ins1*, but we chose the evolutionarily conserved *Ins2* gene due to the greater similarity between *Ins2* and *INS*.[71,100] Furthermore, our prior scRNA-seq analysis revealed a strong correlation between the two insulin genes in mice, and we had also observed similar cell states using an *Ins1* promoter reporter in another previous study.[10,15]

Our 3D imaging showed how the *Ins2*(GFP)^{HIGH} and *Ins2*(GFP)^{LOW} expression states existed in live intact islets. The two *Ins2* gene expression states were present in intact islets. We did not find any correlation for either cell population to the islet periphery or core. This is similar to what was observed by Johnston et al., in which "hub cells," a β cell sub-set with similarities to *Ins2*(GFP)^{LOW} cells, did not show any clear preference for the islet center or periphery.[101] Interestingly, cells in the same activity states were more likely to be next to each other, forming loose patches of cells. Currently, it is unknown why these cells tend to cluster, and future experiments may further explore the spatial dynamics of the two cell states and their relationship with other cells.[102,103]

Previous studies identified the *Ins2*(GFP)^{HIGH} cells as being more mature, producing more *Ins2* mRNA, and more susceptible to stress.[15] The current study characterized the *Ins2*(GFP)^{HIGH} and *Ins2*(GFP)^{LOW} expression states at the proteome level and revealed mechanisms governing *Ins2* gene activity and cell state transitions. Proteomics analysis supported our prior hypothesis that *Ins2*(GFP)^{HIGH} are more mature, including the upregulation of the proliferation repressor RING2. Prior studies have shown that β cells which produce less insulin have increased rates of proliferation.[19] When adjusting for multiple comparisons, we found relatively few proteins that were significantly different in between our samples. This was attributed to the low cell counts

A

	Treatment	Target gene	GFP (at 48 hours)	Cell death (at 72 hours)
cAMP signalling	GLP-1	GLP-1R	4.1	2.5
	IBMX	PDE3A	3.6	1.3
	Pramlintide	CALCR/RAMP3	-0.5	3.9
	SST	SSTR2	-1.0	2.8
	Epinephrine	ADRB1/ADRB2	-3.5	3.3
Calcineurin signalling	Tacrolimus/FK506	PPP3CC	-1.2	2.8
	Cylcosporin A	PPP3CC	-1.3	17.8
	Okadaic	PPP2CA	-3.0	5.5
Endonucleases	APY 29	IRE1A	3.2	29.1
	Sunitinib	INSR/IRE1A	-1.1	47.6
ER pumps and channels	Thapsigargin	ATP2A2	1.1	8.4
	Ryanodine	RYR2	-0.9	1.9
	xestospongin C	ITPR3	-1.6	10.4
Insulin signalling	Staurosporine	PAK1	1.9	1.0
	AICAR	PRKAA2	0.6	3.8
	LY 294002	PIK3CA	1.7	28.9
	Wortmannin	PIK3CA	-0.1	3.0
	AS1842856	FOXO1	-0.2	3.1
	Metformin	PRKAA2	-0.3	2.3
	S961	INSR	-0.5	2.2
	HNMPA	INSR	-1.1	1.4
Nuclear receptors	Rosiglitazone	PPARG	0.7	4.9
	Dexamethasone	NR3C1	-1.5	6.4
Nutrients	Sodium butyrate	SP1	1.6	3.3
	Arginine	NOS1	1.6	3.7
	Palmitate	FFAR1	1.3	7.7
Excitability	Verapamil	CACNA1C	0.2	8.5
	Tolbutamide	SUR1	-0.2	1.8
	Diazoxide	SUR1	-1.3	3.9
Protein degradation	Tunicamycin	GNPTAB/GNPTG	0.2	6.8
	Bortezomib	PSMB5	0.1	3.6
	MG132	PSMB5	-0.6	2.3
	Eeyarestatin I	VCP	-8.5	97.3
Transcription	Triptolide	XPB	3.3	37.4
	α-amanitin	POLR2A	2.6	28.3
	DRB	CDK9	1.9	23.5
	MGCD0103/Mocetinostat	HDAC1/HDAC2	0.6	24.0
	Trichostatin A/TSA	HDAC1	-2.2	8.9
	Actinomycin D	TOP1	-16.8	99.9
Translation factors	Cyclohexamide	EEF2	1.9	35.8
	PKRi/C16	EIF2AK2	1.3	7.8
	Azoramide	EIF2AK3	0.7	4.5
	DHBDC	EIF2AK3	0.4	3.5
	GSK2606414	EIF2AK3	-0.1	3.0
	Sal003	EIF2S1	-0.7	13.4
	ISX-9/Isoxazole 9	AXIN1	-0.8	11.1
	ISRIB	EIF2B1	-0.9	3.8
	CCT020312	EIF2AK3	-0.9	22.7

B

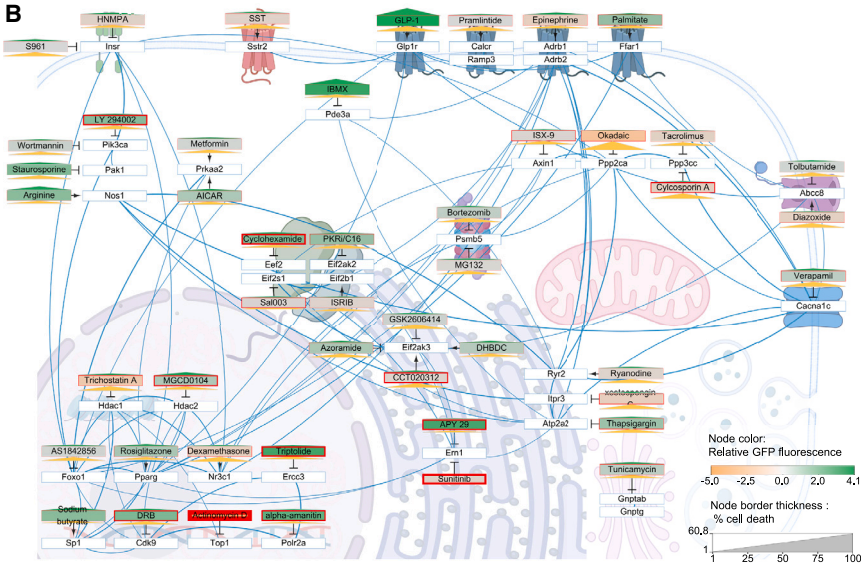

Figure 6. Integration of STRING protein networks and a small molecule screen on Cytoscape

(A) Table of small molecules and their primary target genes. Target genes were identified based on online literature search.

(B) Primary binding partners for small molecules used in the screen localized in Cytoscape. Binding partners (bold) are chosen based on their affinity to the small molecule. Color of the nodes represents GFP fluorescence (scaled) after 48 h of treatment. Borders of the nodes represents cell death (scaled PI fluorescence) after 72 h of treatment. Height of green triangles represents *Ins2*(GFP)^{LOW} to *Ins2*(GFP)^{HIGH} transition rates. Height of orange triangles represents *Ins2*(GFP)^{HIGH} to *Ins2*(GFP)^{LOW} transition rates. Blue lines represent STRING interactions. Pointed arrows with gray lines represent upregulation. Inhibitor arrows with gray lines represent downregulation.

in the *Ins2*(GFP)^{HIGH} state which resulted in high variability between those samples. The low cell counts may result from cell death during cell dispersion and FACS, perhaps worsened by the *Ins2*(GFP)^{HIGH} state's innate fragility.[15] However, strong trends in the dataset prompted us to perform our analysis without adjusting for multiple comparisons. Minimally biased interrogations of proteins and protein networks selectively present in β cells and β cell states build on past efforts to map the β cell proteome. Previously proteomic analysis of FACS purifying mouse β cell populations based on insulin immunoreactivity yielded 6955 proteins across 36 islet samples with various diets and islet cell types[20]; this led to the identification of a subpopulation of β cells with low CD81 expression which had enrichment for factors in spliceosome and RNA processing pathways, but reduced oxidative phosphorylation factors, similar to our *Ins2*(GFP)^{HIGH} cells.[20] Two β cell subpopulations identified in a study on human β cell scRNAseq data had low *INS* expression, and while one high UPR marker expression, the other had enrichment in pathways related to oxidative stress.[8] These two β cell subpopulations possess similarities with our *Ins2*(GFP)^{LOW} cells, which had upregulation in ER stress markers and metabolic processes (Figures S8A–S8C), and it was proposed that these low *INS* expressing cells were in a state of recovery from the various stresses of high insulin production.[8] A recent study investigating younger and older insulin granules in INS-1 cells found proteins such as DYNC1H1, DCTN4, ARHGAP1 and EIF2S2 enriched in younger granules; these proteins were also significantly or trending toward enriched in *Ins2*(GFP)^{LOW} cells, suggesting that the two cell states may have different proportions of young and old insulin granules.[104] Overall, our study identifies novel and previously established β cell markers at the protein level and presented results showing how the cells in a high *Ins2* gene expression state had enrichment for factors related to RNA processing and transcription, with reduced oxidative phosphorylation and ER stress markers.

Our OPP protein translation assay revealed that the *Ins2*(GFP)^{HIGH} state had significantly higher protein synthesis activity. This upregulation of translation could be mediated by an increased abundance of mRNA processing proteins (such as PAPOLA and ZRANB2) and proteins that may play a role in translation (such as DRG1 and ZC3H15) that were detected in

proteomics (Figure S5B). Since our prior study showed that FACS purified *Ins2*(GFP)^{HIGH} cells have upregulated *Ins2* mRNA using qPCR[15] and our scRNAseq data showed that *Ins2* mRNA was the most positively correlated gene with GFP mRNA,[15] this cell state is likely associated with both high insulin transcription and translation. Future studies should look into whether this upregulation in translational capacity is indicative of enhanced insulin secretion capacity.[7,105,106]

Our previous work revealed that cell *Ins2* gene activity was dynamic, and cells in the two cell states may transition between each other.[15] Our targeted perturbation analysis further explores this phenomenon and reveals pathways that impact endogenous *Ins2* gene activity and cell state transitions. A small molecule screen was previously done on live zebrafish larvae, with a set concentration for all treatments.[107] We did not identify overlap between their significant hits and ours, and we speculate this to be a result of the difference between whole organism screens and cell culture screens, as well as possible differences between the organisms involved. While whole organism screens can provide *in vivo* results and minimally perturb the health of biological samples during processing, cell culture screens allow direct interaction between treatments and the target cells. Our results revealed the calcineurin inhibitors tacrolimus, cyclosporine A, and okadaic acid reduced *Ins2* gene activity (Figure 4C), consistent with known roles for calcineurin on insulin mRNA in transgenic mice with a human insulin promoter.[64] Okadaic acid and cyclosporine A are the two top inducers of *Ins2*(GFP)^{HIGH} to *Ins2*(GFP)^{LOW} transitions. NFAT, a calcineurin target, has been reported to be required for the cAMP-mediated upregulation of insulin transcription in INS-1E cells.[108] Interestingly, IRS2, a reported target of calcineurin for the regulation of human β cell survival, is enriched in *Ins2*(GFP)^{HIGH} cells, further supporting a role for calcineurin in cell state regulation.[109]

A key finding of our study was that GLP-1 amide and IBMX robustly increased *Ins2* activity over time, peaking at around 25 h for GLP-1 amide and 55 h for IBMX (Figure 4B). This is consistent with previous data demonstrating that cAMP signaling plays a critical role in insulin production and secretion, with the augmentation of cAMP having significant effects on β cell function and survival.[110–114] GLP-1 has also been shown to increase insulin mRNA and *Ins1* promoter activity in INS-1 insulinoma cell lines, and we now extend these results to the endogenous *Ins2* gene in mice primary cells.[71] Interestingly, GLP-1 and IBMX also had the highest rates of *Ins2*(GFP)^{LOW} to *Ins2*(GFP)^{HIGH} transitions (Figure 5D). Our proteomics analyses revealed that *Ins2*(GFP)^{HIGH} cells had upregulation in two phosphodiesterase (PDE) isoforms, PDE1C and PDE8A, both of which are known to play major roles in regulating cAMP and GSIS in rodent β cells.[115,116] Okadaic acid, the strongest inducer of *Ins2*(GFP)^{HIGH} to *Ins2*(GFP)^{LOW} transitions, is known to increase PDE expression in rat adipocytes.[117] It is also worth noting that despite strongly upregulating GFP expression, many treatments including APY29, triptolide, alpha amanitin, staurosporine, sodium butyrate, and arginine, did not induce nearly as many cell state transitions as IBMX and GLP-1 amide. Taken together, these results may suggest that the dynamics between calcineurin, cAMP, and PDE concentrations play a major role in regulating *Ins2* gene activity and cell state transitions.

Some small molecules had effects on GFP fluorescence that were strongly correlated to cell health. For example, actinomycin D and eeyarestatin I killed cells rapidly upon treatment, resulting in a rapid collapse of GFP fluorescence. Interestingly, a subset of drugs including APY29 (IRE-1A inhibitor), triptolide (TFIIH inhibitor), alpha amanitin (RNA polymerase II inhibitor), cyclohexamide (EEF2 inhibitor), DRB (CDK9 inhibitor), and LY294002 (PI3K inhibitor) induced a strong increase in GFP fluorescence followed by rapid cell death after prolonged treatment. The endonuclease IRE-1A is an important factor in β cell stress regulation[99]; the inhibition of IRE-1A results in increased insulin mRNA content and β cell function, something that we also observe via the increase in GFP after 48 h of inhibition via APY29.[61] The high cell death that follows after this peak in *Ins2* gene activity may be a result of β cell overwork.[19] Inhibition of general transcriptional machinery such as TFIIH and RNA polymerase II is highly detrimental to cell health after prolonged periods of time.[118,119] Inhibition of translation and cell cycle factors are also known to be toxic to cells.[120,121] The PI3K signaling pathway is linked to cell survival and resistance mechanisms.[122] The toxicity of these drugs may result in a buildup of stress cumulating in eventual cell death It is interesting to note that the increase in GFP fluorescence in these drugs only occurs in *Ins2*(GFP)^{HIGH} cells, but not *Ins2*(GFP)^{LOW} cells. This may be due to the inherent fragility in *Ins2*(GFP)^{HIGH} cells, which may make them more vulnerable to the effects of stress.[15] Autofluoresence is also known to increase during the process of cell death, and this may also contribute to the increase in GFP fluorescence.[123] The OPP assay done in the context of several small molecules of interest also supports this, with cells treated to 24 h of triptolide and APY 29 displaying reduced translational capacity prior to cell death and reduction in GFP fluorescence. Furthermore, these molecules all have the capacity to directly influence insulin production through the above stated mechanisms, with most having an inhibitory effect. This may suggest the existence of feedback mechanisms, as the cell tries to replenish insulin mRNA stores through increasing *Ins2* gene activity. These findings may suggest links between cell health and *Ins2* gene activity.

In summary, we provide data that further revealed the differences between the *Ins2*(GFP)^{HIGH} and *Ins2*(GFP)^{LOW} expression states beyond our previous study. Our live cell 3D imaging captured the two cell states in intact living islets, and our proteomic and translational assays characterized them at the protein and functional level. The small molecule screen revealed pathways that may impact *Ins2* gene activity and cell state transitions, including prominent effects by effectors of cAMP signaling. Future studies may further explore the effects of cAMP and calcineurin effectors on *Ins2* gene dynamics and cell state transitions, such as dose response experiments to gauge the thresholds for transitions and the balance between β cell health and function. Studies may also be conducted to explore the cell states in the context of patients with diabetes; it has been shown that some patients with long-term type 1 diabetes still possess β cells which produce low levels of insulin, which may have similarities with our *Ins2*(GFP)^{LOW} cells.[124] Our study highlights the importance of cell expression states and cell state transitions in the islet, and how targeting factors which

influence cell state transitions may help manage β cell function in diabetes.

Limitations of the study

Our study has many limitations, and we list three examples here. First, our 3D imaging experiments were unable to capture the innermost cells in larger intact islets, so we focused mostly on smaller islets. Future experiments could use 2-photon microscopy to analyze islets of varying sizes. Second, as mentioned in the discussion, our proteomics analyses had high variability within sample groups. Future studies should increase the number of biological replicates in proteomics experiments. Third, our small molecule screen started with known compounds with expected effects and is therefore not unbiased. Now that the methodology is established, future studies could examine larger libraries of compounds that cover chemical space in a more unbiased way. Despite these limitations, our study provides new information on primary β cell states and the pathways that control them.

RESOURCE AVAILABILITY

Lead contact

Further information and requests for resources and reagents should be directed to and will be fulfilled by the Lead Contact, James D. Johnson, PhD., 5358 Life Sciences Building, 2350 Health Sciences Mall, University of British Columbia, Vancouver, Canada, V6T 1Z3. Phone: 604 822 7187, Email: James.d.johnson@ubc.ca.

Materials availability

This study did not generate new unique reagents.

Data and code availability

This study did not generate new code.

- Data: Proteomic data are available on ProteomExchange (number PXD052023).
- Code: Coding used in analyses is available upon reasonable request to the authors.
- Other items: Requests for other data are available upon reasonable request to the authors.

ACKNOWLEDGMENTS

We thank many colleagues for helpful discussions during conferences, meetings, and presentations. The research was supported by a CIHR operating grant (PJT152999) to J.D.J., the JDRF Centre of Excellence at UBC (3-COE-2022-1103-*M*-B), and core facilities in the Life Sciences Institute.

AUTHOR CONTRIBUTIONS

CM. J. C. designed studies, performed experiments, analyzed/interpreted data, and wrote the article. B. S. performed experiments, analyzed/interpreted data, and wrote parts of the article. H. H. C. analyzed/interpreted data. X. H. performed experiments. W. G. S. performed experiments. G. P. B. performed experiments and analyzed/interpreted data. Y. H. X. analyzed/interpreted data. J. R. performed experiments, analyzed/interpreted data, wrote parts of article. J. D. J. conceived the project, designed studies, interpreted data, and edited the article. J.D.J. is the guarantor of this work and, as such, had full access to all the data in the study and takes responsibility for the integrity of the data and the accuracy of the data analysis.

DECLARATION OF INTERESTS

The authors declare no competing interests.

STAR★METHODS

Detailed methods are provided in the online version of this paper and include the following:

- KEY RESOURCES TABLE
- EXPERIMENTAL MODEL AND STUDY PARTICIPANT DETAILS
  - Animal husbandry
- METHOD DETAILS
  - Islet isolation and dissociation
  - Fluorescence-activated cell sorting
  - Live cell imaging and analysis
  - Protein synthesis assay
  - Mass spectrometry/proteomics
- QUANTIFICATION AND STATISTICAL ANALYSIS
  - Statistics and data visualization

SUPPLEMENTAL INFORMATION

Supplemental information can be found online at https://doi.org/10.1016/j.isci.2025.112015.

Received: August 30, 2024
Revised: November 19, 2024
Accepted: February 10, 2025
Published: February 17, 2025

REFERENCES

1. Tisch, R., and McDevitt, H. (1996). Insulin-dependent diabetes mellitus. Cell *85*, 291–297. https://doi.org/10.1016/s0092-8674(00)81106-x.
2. Boland, B.B., Rhodes, C.J., and Grimsby, J.S. (2017). The dynamic plasticity of insulin production in beta-cells. Mol. Metab. *6*, 958–973. https://doi.org/10.1016/j.molmet.2017.04.010.
3. Butler, A.E., Janson, J., Bonner-Weir, S., Ritzel, R., Rizza, R.A., and Butler, P.C. (2003). Beta-cell deficit and increased beta-cell apoptosis in humans with type 2 diabetes. Diabetes *52*, 102–110. https://doi.org/10.2337/diabetes.52.1.102.
4. Brozzi, F., and Eizirik, D.L. (2016). ER stress and the decline and fall of pancreatic beta cells in type 1 diabetes. Upsala J. Med. Sci. *121*, 133–139. https://doi.org/10.3109/03009734.2015.1135217.
5. Avrahami, D., Klochendler, A., Dor, Y., and Glaser, B. (2017). Beta cell heterogeneity: an evolving concept. Diabetologia *60*, 1363–1369. https://doi.org/10.1007/s00125-017-4326-z.
6. Gutierrez, G.D., Gromada, J., and Sussel, L. (2017). Heterogeneity of the Pancreatic Beta Cell. Front. Genet. *8*, 9.
7. Dorrell, C., Schug, J., Canaday, P.S., Russ, H.A., Tarlow, B.D., Grompe, M.T., Horton, T., Hebrok, M., Streeter, P.R., Kaestner, K.H., and Grompe, M. (2016). Human islets contain four distinct subtypes of beta cells. Nat. Commun. *7*, 11756. https://doi.org/10.1038/ncomms11756.
8. Xin, Y., Dominguez Gutierrez, G., Okamoto, H., Kim, J., Lee, A.H., Adler, C., Ni, M., Yancopoulos, G.D., Murphy, A.J., and Gromada, J. (2018). Pseudotime Ordering of Single Human beta-Cells Reveals States of Insulin Production and Unfolded Protein Response. Diabetes *67*, 1783–1794. https://doi.org/10.2337/db18-0365.
9. Farack, L., Golan, M., Egozi, A., Dezorella, N., Bahar Halpern, K., Ben-Moshe, S., Garzilli, I., Tóth, B., Roitman, L., Krizhanovsky, V., and Itzkovitz, S. (2019). Transcriptional Heterogeneity of Beta Cells in the Intact Pancreas. Dev. Cell *48*, 115–125.e4. https://doi.org/10.1016/j.devcel.2018.11.001.

10. Szabat, M., Luciani, D.S., Piret, J.M., and Johnson, J.D. (2009). Maturation of adult beta-cells revealed using a Pdx1/insulin dual-reporter lentivirus. Endocrinology *150*, 1627–1635. https://doi.org/10.1210/en.2008-1224.

11. Szabat, M., Pourghaderi, P., Soukhatcheva, G., Verchere, C.B., Warnock, G.L., Piret, J.M., and Johnson, J.D. (2011). Kinetics and genomic profiling of adult human and mouse beta-cell maturation. Islets *3*, 175–187. https://doi.org/10.4161/isl.3.4.15881.

12. Szabat, M., Johnson, J.D., and Piret, J.M. (2010). Reciprocal modulation of adult beta cell maturity by activin A and follistatin. Diabetologia *53*, 1680–1689. https://doi.org/10.1007/s00125-010-1758-0.

13. Szabat, M., Modi, H., Ramracheya, R., Girbinger, V., Chan, F., Lee, J.T.C., Piske, M., Kamal, S., Carol Yang, Y.H., Welling, A., et al. (2015). High-content screening identifies a role for Na(+) channels in insulin production. R. Soc. Open Sci. *2*, 150306. https://doi.org/10.1098/rsos.150306.

14. Wakae-Takada, N., Xuan, S., Watanabe, K., Meda, P., and Leibel, R.L. (2013). Molecular basis for the regulation of islet beta cell mass in mice: the role of E-cadherin. Diabetologia *56*, 856–866. https://doi.org/10.1007/s00125-012-2824-6.

15. Chu, C.M.J., Modi, H., Ellis, C., Krentz, N.A.J., Skovsø, S., Zhao, Y.B., Cen, H., Noursadeghi, N., Panzhinskiy, E., Hu, X., et al. (2022). Dynamic Ins2 Gene Activity Defines beta-Cell Maturity States. Diabetes *71*, 2612–2631. https://doi.org/10.2337/db21-1065.

16. Kolic, J.,S.G., Cen, H.H., Ewald, J., Beet, L., Moravcova, R., Rogalski, J.C., Sasaki, S., Sun, H., Rajesh, V., Xia, Y.H., et al. (2024). Proteomic predictors of individualized nutrient-specific insulin secretion in health and disease. Cell Metab. *36*, 1619–1633.e5.

17. Hershey, J.W.B., Sonenberg, N., and Mathews, M.B. (2012). Principles of translational control: an overview. Cold Spring Harb. Perspect. Biol. *4*, a011528. https://doi.org/10.1101/cshperspect.a011528.

18. Spriggs, K.A., Bushell, M., and Willis, A.E. (2010). Translational regulation of gene expression during conditions of cell stress. Mol. Cell *40*, 228–237. https://doi.org/10.1016/j.molcel.2010.09.028.

19. Szabat, M., Page, M.M., Panzhinskiy, E., Skovsø, S., Mojibian, M., Fernandez-Tajes, J., Bruin, J.E., Bround, M.J., Lee, J.T.C., Xu, E.E., et al. (2016). Reduced Insulin Production Relieves Endoplasmic Reticulum Stress and Induces beta Cell Proliferation. Cell Metab. *23*, 179–193. https://doi.org/10.1016/j.cmet.2015.10.016.

20. Fu, Q., Jiang, H., Qian, Y., Lv, H., Dai, H., Zhou, Y., Chen, Y., He, Y., Gao, R., Zheng, S., et al. (2023). Single-cell RNA sequencing combined with single-cell proteomics identifies the metabolic adaptation of islet cell subpopulations to high-fat diet in mice. Diabetologia *66*, 724–740. https://doi.org/10.1007/s00125-022-05849-5.

21. Brackeva, B., Kramer, G., Vissers, J.P.C., and Martens, G.A. (2015). Quantitative proteomics of rat and human pancreatic beta cells. Data Brief *3*, 234–239. https://doi.org/10.1016/j.dib.2015.02.019.

22. Cui, Y.F., Ma, M., Wang, G.Y., Han, D.E., Vollmar, B., and Menger, M.D. (2005). Prevention of core cell damage in isolated islets of Langerhans by low temperature preconditioning. World J. Gastroenterol. *11*, 545–550. https://doi.org/10.3748/wjg.v11.i4.545.

23. Brownrigg, G.P., Xia, Y.H., Chu, C.M.J., Wang, S., Chao, C., Zhang, J.A., Skovsø, S., Panzhinskiy, E., Hu, X., Johnson, J.D., and Rideout, E.J. (2023). Sex differences in islet stress responses support female beta cell resilience. Mol. Metab. *69*, 101678. https://doi.org/10.1016/j.molmet.2023.101678.

24. Jain, C., Lickert, H., Bilekova, S., and Bilekova, S. (2022). Targeting pancreatic beta cells for diabetes treatment. Nat. Metab. *4*, 1097–1108. https://doi.org/10.1038/s42255-022-00618-5.

25. Martens, G.A., Jiang, L., Hellemans, K.H., Stangé, G., Heimberg, H., Nielsen, F.C., Sand, O., Van Helden, J., Van Lommel, L., Schuit, F., et al. (2011). Clusters of conserved beta cell marker genes for assessment of beta cell phenotype. PLoS One *6*, e24134. https://doi.org/10.1371/journal.pone.0024134.

26. Horn, S., Kirkegaard, J.S., Hoelper, S., Seymour, P.A., Rescan, C., Nielsen, J.H., Madsen, O.D., Jensen, J.N., Krüger, M., Grønborg, M., and Ahnfelt-Rønne, J. (2016). Research Resource: A Dual Proteomic Approach Identifies Regulated Islet Proteins During beta-Cell Mass Expansion In Vivo. Mol. Endocrinol. *30*, 133–143. https://doi.org/10.1210/me.2015-1208.

27. van Gurp, L., Fodoulian, L., Oropeza, D., Furuyama, K., Bru-Tari, E., Vu, A.N., Kaddis, J.S., Rodríguez, I., Thorel, F., and Herrera, P.L. (2022). Generation of human islet cell type-specific identity genesets. Nat. Commun. *13*, 2020. https://doi.org/10.1038/s41467-022-29588-8.

28. Kim, B.M., Han, Y.M., Shin, Y.J., Min, B.H., and Park, I.S. (2001). Clusterin expression during regeneration of pancreatic islet cells in streptozotocin-induced diabetic rats. Diabetologia *44*, 2192–2202. https://doi.org/10.1007/s001250100029.

29. Camunas-Soler, J., Dai, X.Q., Hang, Y., Bautista, A., Lyon, J., Suzuki, K., Kim, S.K., Quake, S.R., and MacDonald, P.E. (2020). Patch-Seq Links Single-Cell Transcriptomes to Human Islet Dysfunction in Diabetes. Cell Metab. *31*, 1017–1031.e4. https://doi.org/10.1016/j.cmet.2020.04.005.

30. Mugabo, Y., Zhao, C., Tan, J.J., Ghosh, A., Campbell, S.A., Fadzeyeva, E., Paré, F., Pan, S.S., Galipeau, M., Ast, J., et al. (2022). 14-3-3zeta Constrains insulin secretion by regulating mitochondrial function in pancreatic beta cells. JCI Insight *7*, e156378. https://doi.org/10.1172/jci.insight.156378.

31. Cruciani-Guglielmacci, C., Meneyrol, K., Denom, J., Kassis, N., Rachdi, L., Makaci, F., Migrenne-Li, S., Daubigney, F., Georgiadou, E., Denis, R.G., et al. (2022). Homocysteine Metabolism Pathway Is Involved in the Control of Glucose Homeostasis: A Cystathionine Beta Synthase Deficiency Study in Mouse. Cells *11*, 1737. https://doi.org/10.3390/cells11111737.

32. Laboute, T., Zucca, S., Holcomb, M., Patil, D.N., Garza, C., Wheatley, B.A., Roy, R.N., Forli, S., and Martemyanov, K.A. (2023). Orphan receptor GPR158 serves as a metabotropic glycine receptor: mGlyR. Science *379*, 1352–1358. https://doi.org/10.1126/science.add7150.

33. Yan-Do, R., Duong, E., Manning Fox, J.E., Dai, X., Suzuki, K., Khan, S., Bautista, A., Ferdaoussi, M., Lyon, J., Wu, X., et al. (2016). A Glycine-Insulin Autocrine Feedback Loop Enhances Insulin Secretion From Human β-Cells and Is Impaired in Type 2 Diabetes. Diabetes *65*, 2311–2321. https://doi.org/10.2337/db15-1272.

34. Alam, C.M., Silvander, J.S.G., Daniel, E.N., Tao, G.Z., Kvarnström, S.M., Alam, P., Omary, M.B., Hänninen, A., and Toivola, D.M. (2013). Keratin 8 modulates beta-cell stress responses and normoglycaemia. J. Cell Sci. *126*, 5635–5644. https://doi.org/10.1242/jcs.132795.

35. Weidemann, B.J., Marcheva, B., Kobayashi, M., Omura, C., Newman, M.V., Kobayashi, Y., Waldeck, N.J., Perelis, M., Lantier, L., McGuinness, O.P., et al. (2024). Repression of latent NF-kappaB enhancers by PDX1 regulates beta cell functional heterogeneity. Cell Metab. *36*, 90–102.e107. https://doi.org/10.1016/j.cmet.2023.11.018.

36. Mellado-Gil, J.M., Fuente-Martín, E., Lorenzo, P.I., Cobo-Vuilleumier, N., López-Noriega, L., Martín-Montalvo, A., Gómez, I.d.G.H., Ceballos-Chávez, M., Gómez-Jaramillo, L., Campos-Caro, A., et al. (2018). The type 2 diabetes-associated HMG20A gene is mandatory for islet beta cell functional maturity. Cell Death Dis. *9*, 279. https://doi.org/10.1038/s41419-018-0272-z.

37. Pan, L., Hu, Y., Qian, C., Yao, Y., Wang, S., Shi, W., and Xu, T. (2022). RNF2 mediates pulmonary fibroblasts activation and proliferation by regulating mTOR and p16-CDK4-Rb1 signaling pathway. Inflamm. Res. *71*, 1283–1303. https://doi.org/10.1007/s00011-022-01617-8.

38. Muraro, M.J., Dharmadhikari, G., Grun, D., Groen, N., Dielen, T., Jansen, E., van Gurp, L., Engelse, M.A., Carlotti, F., de Koning, E.J., and van Oudenaarden, A. (2016). A Single-Cell Transcriptome Atlas of the Human

Pancreas. Cell Syst. *3*, 385–394.e383. https://doi.org/10.1016/j.cels.2016.09.002.

39. Baker, M.J., Webb, C.T., Stroud, D.A., Palmer, C.S., Frazier, A.E., Guiard, B., Chacinska, A., Gulbis, J.M., and Ryan, M.T. (2009). Structural and functional requirements for activity of the Tim9-Tim10 complex in mitochondrial protein import. Mol. Biol. Cell *20*, 769–779. https://doi.org/10.1091/mbc.e08-09-0903.

40. Jayaram, B., and Kowluru, A. (2012). Phagocytic NADPH oxidase links ARNO-Arf6 signaling pathway in glucose-stimulated insulin secretion from the pancreatic beta-cell. Cell. Physiol. Biochem. *30*, 1351–1362. https://doi.org/10.1159/000343324.

41. Rodriguez-Agudo, D., Malacrida, L., Kakiyama, G., Sparrer, T., Fortes, C., Maceyka, M., Subler, M.A., Windle, J.J., Gratton, E., Pandak, W.M., and Gil, G. (2019). StarD5: an ER stress protein regulates plasma membrane and intracellular cholesterol homeostasis. J. Lipid Res. *60*, 1087–1098. https://doi.org/10.1194/jlr.M091967.

42. Pelligra, A., Mrugala, J., Griess, K., Kirschner, P., Nortmann, O., Bartosinska, B., Köster, A., Krupenko, N.I., Gebel, D., Westhoff, P., et al. (2023). Pancreatic islet protection at the expense of secretory function involves serine-linked mitochondrial one-carbon metabolism. Cell Rep. *42*, 112703. https://doi.org/10.1016/j.celrep.2023.112703.

43. Noordstra, I., van den Berg, C.M., Boot, F.W.J., Katrukha, E.A., Yu, K.L., Tas, R.P., Portegies, S., Viergever, B.J., de Graaff, E., Hoogenraad, C.C., et al. (2022). Organization and dynamics of the cortical complexes controlling insulin secretion in beta-cells. J. Cell Sci. *135*, jcs259430. https://doi.org/10.1242/jcs.259430.

44. Mziaut, H., Mulligan, B., Hoboth, P., Otto, O., Ivanova, A., Herbig, M., Schumann, D., Hildebrandt, T., Dehghany, J., Sönmez, A., et al. (2016). The F-actin modifier villin regulates insulin granule dynamics and exocytosis downstream of islet cell autoantigen 512. Mol. Metab. *5*, 656–668. https://doi.org/10.1016/j.molmet.2016.05.015.

45. Moss, N.D., Wells, K.L., Theis, A., Kim, Y.K., Spigelman, A.F., Liu, X., MacDonald, P.E., and Sussel, L. (2023). Modulation of insulin secretion by RBFOX2-mediated alternative splicing. Nat. Commun. *14*, 7732. https://doi.org/10.1038/s41467-023-43605-4.

46. Liu, X., Yan, F., Yao, H., Chang, M., Qin, J., Li, Y., Wang, Y., and Pei, X. (2014). Involvement of RhoA/ROCK in insulin secretion of pancreatic beta-cells in 3D culture. Cell Tissue Res. *358*, 359–369. https://doi.org/10.1007/s00441-014-1961-2.

47. Johnson, J.D., Bernal-Mizrachi, E., Alejandro, E.U., Han, Z., Kalynyak, T.B., Li, H., Beith, J.L., Gross, J., Warnock, G.L., Townsend, R.R., et al. (2006). Insulin protects islets from apoptosis via Pdx1 and specific changes in the human islet proteome. Proc. Natl. Acad. Sci. USA *103*, 19575–19580. https://doi.org/10.1073/pnas.0604208103.

48. Loughlin, F.E., Mansfield, R.E., Vaz, P.M., McGrath, A.P., Setiyaputra, S., Gamsjaeger, R., Chen, E.S., Morris, B.J., Guss, J.M., and Mackay, J.P. (2009). The zinc fingers of the SR-like protein ZRANB2 are single-stranded RNA-binding domains that recognize 5' splice site-like sequences. Proc. Natl. Acad. Sci. USA *106*, 5581–5586. https://doi.org/10.1073/pnas.0802466106.

49. Colwill, K., Feng, L.L., Yeakley, J.M., Gish, G.D., Cáceres, J.F., Pawson, T., and Fu, X.D. (1996). SRPK1 and Clk/Sty protein kinases show distinct substrate specificities for serine/arginine-rich splicing factors. J. Biol. Chem. *271*, 24569–24575. https://doi.org/10.1074/jbc.271.40.24569.

50. Thuresson, A.C., Aström, J., Aström, A., Grönvik, K.O., and Virtanen, A. (1994). Multiple forms of poly(A) polymerases in human cells. Proc. Natl. Acad. Sci. USA *91*, 979–983. https://doi.org/10.1073/pnas.91.3.979.

51. Hobson, B.D., Kong, L., Hartwick, E.W., Gonzalez, R.L., and Sims, P.A. (2020). Elongation inhibitors do not prevent the release of puromycylated nascent polypeptide chains from ribosomes. Elife *9*, e60048. https://doi.org/10.7554/eLife.60048.

52. Batista, G., Johnson, J.L., Dominguez, E., Costa-Mattioli, M., and Pena, J.L. (2016). Translational control of auditory imprinting and structural plasticity by eIF2α. Elife *5*, e17197. https://doi.org/10.7554/eLife.17197.

53. Bruch, J., Xu, H., Rösler, T.W., De Andrade, A., Kuhn, P.H., Lichtenthaler, S.F., Arzberger, T., Winklhofer, K.F., Müller, U., and Höglinger, G.U. (2017). PERK activation mitigates tau pathology *in vitro* and *in vivo*. EMBO Mol. Med. *9*, 371–384. https://doi.org/10.15252/emmm.201606664.

54. Bai, H., Chen, T., Ming, J., Sun, H., Cao, P., Fusco, D.N., Chung, R.T., Chorev, M., Jin, Q., and Aktas, B.H. (2013). Dual activators of protein kinase R (PKR) and protein kinase R-like kinase PERK identify common and divergent catalytic targets. Chembiochem *14*, 1255–1262. https://doi.org/10.1002/cbic.201300177.

55. Sekine, Y., Zyryanova, A., Crespillo-Casado, A., Fischer, P.M., Harding, H.P., and Ron, D. (2015). Stress responses. Mutations in a translation initiation factor identify the target of a memory-enhancing compound. Science *348*, 1027–1030. https://doi.org/10.1126/science.aaa6986.

56. Axten, J.M., Medina, J.R., Feng, Y., Shu, A., Romeril, S.P., Grant, S.W., Li, W.H.H., Heerding, D.A., Minthorn, E., Mencken, T., et al. (2012). Discovery of 7-methyl-5-(1-{[3-(trifluoromethyl)phenyl]acetyl}-2,3-dihydro-1H-indol-5-yl)-7H-pyrrolo[2,3-d]pyrimidin-4-amine (GSK2606414), a potent and selective first-in-class inhibitor of protein kinase R (PKR)-like endoplasmic reticulum kinase (PERK). J. Med. Chem. *55*, 7193–7207. https://doi.org/10.1021/jm300713s.

57. Christ, W., Tynell, J., and Klingström, J. (2020). Puumala and Andes Orthohantaviruses Cause Transient Protein Kinase R-Dependent Formation of Stress Granules. J. Virol. *94*, 10–1128. https://doi.org/10.1128/JVI.01168-19.

58. Brownrigg, G.P., Xia, Y.H., Chu, C.M.J., Wang, S., Chao, C., Zhang, J.A., Skovsø, S., Panzhinskiy, E., Hu, X., Johnson, J.D., and Rideout, E.J. (2023). Sex differences in islet stress responses support female β cell resilience. Mol. Metab. *69*, 101678. https://doi.org/10.1016/j.molmet.2023.101678.

59. Šereš, M., Pavlíková, L., Boháčová, V., Kyca, T., Borovská, I., Lakatoš, B., Breier, A., and Sulová, Z. (2020). Overexpression of GRP78/BiP in P-Glycoprotein-Positive L1210 Cells is Responsible for Altered Response of Cells to Tunicamycin as a Stressor of the Endoplasmic Reticulum. Cells *9*, 890. https://doi.org/10.3390/cells9040890.

60. Wang, Q., Shinkre, B.A., Lee, J.G., Weniger, M.A., Liu, Y., Chen, W., Wiestner, A., Trenkle, W.C., and Ye, Y. (2010). The ERAD inhibitor Eeyarestatin I is a bifunctional compound with a membrane-binding domain and a p97/VCP inhibitory group. PLoS One *5*, e15479. https://doi.org/10.1371/journal.pone.0015479.

61. Ghosh, R., Wang, L., Wang, E.S., Perera, B.G.K., Igbaria, A., Morita, S., Prado, K., Thamsen, M., Caswell, D., Macias, H., et al. (2014). Allosteric inhibition of the IRE1alpha RNase preserves cell viability and function during endoplasmic reticulum stress. Cell *158*, 534–548. https://doi.org/10.1016/j.cell.2014.07.002.

62. Lutz, S.Z., Ullrich, A., Häring, H.U., Ullrich, S., and Gerst, F. (2017). Sunitinib specifically augments glucose-induced insulin secretion. Cell. Signal. *36*, 91–97. https://doi.org/10.1016/j.cellsig.2017.04.018.

63. Fu, S., Yalcin, A., Lee, G.Y., Li, P., Fan, J., Arruda, A.P., Pers, B.M., Yilmaz, M., Eguchi, K., and Hotamisligil, G.S. (2015). Phenotypic assays identify azoramide as a small-molecule modulator of the unfolded protein response with antidiabetic activity. Sci. Transl. Med. *7*, 292ra98. https://doi.org/10.1126/scitranslmed.aaa9134.

64. Oetjen, E., Baun, D., Beimesche, S., Krause, D., Cierny, I., Blume, R., Dickel, C., Wehner, S., and Knepel, W. (2003). Inhibition of human insulin gene transcription by the immunosuppressive drugs cyclosporin A and tacrolimus in primary, mature islets of transgenic mice. Mol. Pharmacol. *63*, 1289–1295. https://doi.org/10.1124/mol.63.6.1289.

65. Beith, J.L., Alejandro, E.U., and Johnson, J.D. (2008). Insulin stimulates primary beta-cell proliferation via Raf-1 kinase. Endocrinology *149*, 2251–2260. https://doi.org/10.1210/en.2007-1557.

66. Gao, Z., Konrad, R.J., Collins, H., Matschinsky, F.M., Rothenberg, P.L., and Wolf, B.A. (1996). Wortmannin inhibits insulin secretion in pancreatic islets and beta-TC3 cells independent of its inhibition of phosphatidylinositol 3-kinase. Diabetes *45*, 854–862. https://doi.org/10.2337/diab.45.7.854.

67. Powers, A.C., Philippe, J., Hermann, H., and Habener, J.F. (1988). Sodium butyrate increases glucagon and insulin gene expression by recruiting immunocytochemically negative cells to produce hormone. Diabetes *37*, 1405–1410. https://doi.org/10.2337/diab.37.10.1405.

68. Tiernan, A.R., Champion, J.A., and Sambanis, A. (2015). Trichostatin A affects the secretion pathways of beta and intestinal endocrine cells. Exp. Cell Res. *330*, 212–221. https://doi.org/10.1016/j.yexcr.2014.09.031.

69. Fournel, M., Bonfils, C., Hou, Y., Yan, P.T., Trachy-Bourget, M.C., Kalita, A., Liu, J., Lu, A.H., Zhou, N.Z., Robert, M.F., et al. (2008). MGCD0103, a novel isotype-selective histone deacetylase inhibitor, has broad spectrum antitumor activity in vitro and in vivo. Mol. Cancer Ther. *7*, 759–768. https://doi.org/10.1158/1535-7163.MCT-07-2026.

70. Redmon, J.B., Towle, H.C., and Robertson, R.P. (1994). Regulation of human insulin gene transcription by glucose, epinephrine, and somatostatin. Diabetes *43*, 546–551. https://doi.org/10.2337/diab.43.4.546.

71. Skoglund, G., Hussain, M.A., and Holz, G.G. (2000). Glucagon-like peptide 1 stimulates insulin gene promoter activity by protein kinase A-independent activation of the rat insulin I gene cAMP response element. Diabetes *49*, 1156–1164. https://doi.org/10.2337/diabetes.49.7.1156.

72. Schinner, S., Krätzner, R., Baun, D., Dickel, C., Blume, R., and Oetjen, E. (2009). Inhibition of human insulin gene transcription by peroxisome proliferator-activated receptor gamma and thiazolidinedione oral antidiabetic drugs. Br. J. Pharmacol. *157*, 736–745. https://doi.org/10.1111/j.1476-5381.2009.00208.x.

73. Shinozuka, Y., Okada, M., Yasuda, N., and Yokoyama, K.K. (2003). Staurosporine stimulates insulin gene expression via CRE dependent manner. In Nucleic acids symposium series (Oxford University Press), pp. 301–302. https://doi.org/10.1093/nass/3.1.301.

74. Ammälä, C., Eliasson, L., Bokvist, K., Berggren, P.O., Honkanen, R.E., Sjöholm, A., and Rorsman, P. (1994). Activation of protein kinases and inhibition of protein phosphatases play a central role in the regulation of exocytosis in mouse pancreatic beta cells. Proc. Natl. Acad. Sci. USA *91*, 4343–4347. https://doi.org/10.1073/pnas.91.10.4343.

75. Hagman, D.K., Hays, L.B., Parazzoli, S.D., and Poitout, V. (2005). Palmitate inhibits insulin gene expression by altering PDX-1 nuclear localization and reducing MafA expression in isolated rat islets of Langerhans. J. Biol. Chem. *280*, 32413–32418. https://doi.org/10.1074/jbc.M506000200.

76. Moon, J.S., Karunakaran, U., Elumalai, S., Lee, I.K., Lee, H.W., Kim, Y.W., and Won, K.C. (2017). Metformin prevents glucotoxicity by alleviating oxidative and ER stress-induced CD36 expression in pancreatic beta cells. J. Diabet. Complicat. *31*, 21–30. https://doi.org/10.1016/j.jdiacomp.2016.09.001.

77. Parvin, R., Saito-Hakoda, A., Shimada, H., Shimizu, K., Noro, E., Iwasaki, Y., Fujiwara, K., Yokoyama, A., and Sugawara, A. (2017). Role of NeuroD1 on the negative regulation of Pomc expression by glucocorticoid. PLoS One *12*, e0175435. https://doi.org/10.1371/journal.pone.0175435.

78. Dioum, E.M., Osborne, J.K., Goetsch, S., Russell, J., Schneider, J.W., and Cobb, M.H. (2011). A small molecule differentiation inducer increases insulin production by pancreatic β cells. Proc. Natl. Acad. Sci. USA *108*, 20713–20718. https://doi.org/10.1073/pnas.1118526109.

79. Zou, P., Liu, L., Zheng, L., Liu, L., Stoneman, R.E., Cho, A., Emery, A., Gilbert, E.R., and Cheng, Z. (2014). Targeting FoxO1 with AS1842856 suppresses adipogenesis. Cell Cycle *13*, 3759–3767. https://doi.org/10.4161/15384101.2014.965977.

80. Ma, Z., Portwood, N., Brodin, D., Grill, V., and Björklund, A. (2007). Effects of diazoxide on gene expression in rat pancreatic islets are largely linked to elevated glucose and potentially serve to enhance beta-cell sensitivity. Diabetes *56*, 1095–1106. https://doi.org/10.2337/db06-0322.

81. Christie, M.R., and Ashcroft, S.J. (1984). Cyclic AMP-dependent protein phosphorylation and insulin secretion in intact islets of Langerhans. Biochem. J. *218*, 87–99. https://doi.org/10.1042/bj2180087.

82. Leiss, V., Flockerzie, K., Novakovic, A., Rath, M., Schönsiegel, A., Birnbaumer, L., Schürmann, A., Harteneck, C., and Nürnberg, B. (2014). Insulin secretion stimulated by L-arginine and its metabolite L-ornithine depends on Gα(i2). Am. J. Physiol. Endocrinol. Metab. *307*, E800–E812. https://doi.org/10.1152/ajpendo.00337.2014.

83. Devis, G., Somers, G., Van Obberghen, E., and Malaisse, W.J. (1975). Calcium antagonists and islet function. I. Inhibition of insulin release by verapamil. Diabetes *24*, 247–251. https://doi.org/10.2337/diabetes.24.6.247.

84. Johnson, J.D., Kuang, S., Misler, S., and Polonsky, K.S. (2004). Ryanodine receptors in human pancreatic beta cells: localization and effects on insulin secretion. FASEB J. *18*, 878–880. https://doi.org/10.1096/fj.03-1280fje.

85. Wang, C.Z., Wang, Y., Di, A., Magnuson, M.A., Ye, H., Roe, M.W., Nelson, D.J., Bell, G.I., and Philipson, L.H. (2005). 5-amino-imidazole carboxamide riboside acutely potentiates glucose-stimulated insulin secretion from mouse pancreatic islets by KATP channel-dependent and -independent pathways. Biochem. Biophys. Res. Commun. *330*, 1073–1079. https://doi.org/10.1016/j.bbrc.2005.03.093.

86. Suzuki, S., Murakami, M., Abe, S., Satoh, Y., Shintani, S., Ishizuka, J., Suzuki, K., Thompson, J.C., and Toyota, T. (1992). The effects of amylin on insulin secretion from Rin m5F cells and glycogen synthesis and lipogenesis in rat primary cultured hepatocytes. Diabetes Res. Clin. Pract. *15*, 77–84. https://doi.org/10.1016/0168-8227(92)90071-x.

87. Henquin, J.C. (1980). Tolbutamide stimulation and inhibition of insulin release: studies of the underlying ionic mechanisms in isolated rat islets. Diabetologia *18*, 151–160. https://doi.org/10.1007/BF00290493.

88. Stamateris, R.E., Sharma, R.B., Kong, Y., Ebrahimpour, P., Panday, D., Ranganath, P., Zou, B., Levitt, H., Parambil, N.A., O'Donnell, C.P., et al. (2016). Glucose Induces Mouse β-Cell Proliferation via IRS2, MTOR, and Cyclin D2 but Not the Insulin Receptor. Diabetes *65*, 981–995. https://doi.org/10.2337/db15-0529.

89. Schewe, D.M., and Aguirre-Ghiso, J.A. (2009). Inhibition of eIF2alpha dephosphorylation maximizes bortezomib efficiency and eliminates quiescent multiple myeloma cells surviving proteasome inhibitor therapy. Cancer Res. *69*, 1545–1552. https://doi.org/10.1158/0008-5472.CAN-08-3858.

90. Bito, M., Tomita, T., Komori, M., Taogoshi, T., Kimura, Y., and Kihira, K. (2013). The mechanisms of insulin secretion and calcium signaling in pancreatic β-cells exposed to fluoroquinolones. Biol. Pharm. Bull. *36*, 31–35. https://doi.org/10.1248/bpb.b12-00425.

91. Bensaude, O. (2011). Inhibiting eukaryotic transcription: Which compound to choose? How to evaluate its activity? Transcription. Transcription *2*, 103–108. https://doi.org/10.4161/trns.2.3.16172.

92. Stellrecht, C.M., and Chen, L.S. (2011). Transcription inhibition as a therapeutic target for cancer. Cancers *3*, 4170–4190. https://doi.org/10.3390/cancers3044170.

93. Wiegard, A., Kuzin, V., Cameron, D.P., Grosser, J., Ceribelli, M., Mehmood, R., Ballarino, R., Valant, F., Grochowski, R., Karabogdan, I., et al. (2021). Topoisomerase 1 activity during mitotic transcription favors the transition from mitosis to G1. Mol. Cell *81*, 5007–5024.e9. https://doi.org/10.1016/j.molcel.2021.10.015.

94. Bacon, C.W., and D'Orso, I. (2019). CDK9: a signaling hub for transcriptional control. Transcription *10*, 57–75. https://doi.org/10.1080/21541264.2018.1523668.

95. Liu, X., Bushnell, D.A., and Kornberg, R.D. (2013). RNA polymerase II transcription: structure and mechanism. Biochim. Biophys. Acta *1829*, 2–8. https://doi.org/10.1016/j.bbagrm.2012.09.003.

96. Fukuda, A., Nogi, Y., and Hisatake, K. (2002). The regulatory role for the ERCC3 helicase of general transcription factor TFIIH during promoter escape in transcriptional activation. Proc. Natl. Acad. Sci. USA *99*, 1206–1211. https://doi.org/10.1073/pnas.251674198.

97. Gallinari, P., Di Marco, S., Jones, P., Pallaoro, M., and Steinkühler, C. (2007). HDACs, histone deacetylation and gene transcription: from molecular biology to cancer therapeutics. Cell Res. *17*, 195–211. https://doi.org/10.1038/sj.cr.7310149.

98. O'Connor, L., Gilmour, J., and Bonifer, C. (2016). The Role of the Ubiquitously Expressed Transcription Factor Sp1 in Tissue-specific Transcriptional Regulation and in Disease. Yale J. Biol. Med. *89*, 513–525.

99. Chen, Y., and Brandizzi, F. (2013). IRE1: ER stress sensor and cell fate executor. Trends Cell Biol. *23*, 547–555. https://doi.org/10.1016/j.tcb.2013.06.005.

100. Leibiger, B., Moede, T., Uhles, S., Berggren, P.O., and Leibiger, I.B. (2002). Short-term regulation of insulin gene transcription. Biochem. Soc. Trans. *30*, 312–317.

101. Johnston, N.R., Mitchell, R.K., Haythorne, E., Pessoa, M.P., Semplici, F., Ferrer, J., Piemonti, L., Marchetti, P., Bugliani, M., Bosco, D., et al. (2016). Beta Cell Hubs Dictate Pancreatic Islet Responses to Glucose. Cell Metab. *24*, 389–401. https://doi.org/10.1016/j.cmet.2016.06.020.

102. Kim, A., Miller, K., Jo, J., Kilimnik, G., Wojcik, P., and Hara, M. (2009). Islet architecture: A comparative study. Islets *1*, 129–136. https://doi.org/10.4161/isl.1.2.9480.

103. Chabosseau, P., Yong, F., Delgadillo-Silva, L.F., Lee, E.Y., Melhem, R., Li, S., Gandhi, N., Wastin, J., Noriega, L.L., Leclerc, I., et al. (2023). Molecular phenotyping of single pancreatic islet leader beta cells by "Flash-Seq". Life Sci. *316*, 121436. https://doi.org/10.1016/j.lfs.2023.121436.

104. Neukam, M., Sala, P., Brunner, A.D., Ganß, K., Palladini, A., Grzybek, M., Topcheva, O., Vasiljević, J., Broichhagen, J., Johnsson, K., et al. (2024). Purification of time-resolved insulin granules reveals proteomic and lipidomic changes during granule aging. Cell Rep. *43*, 113836. https://doi.org/10.1016/j.celrep.2024.113836.

105. Dror, E., Fagnocchi, L., Wegert, V., Apostle, S., Grimaldi, B., Gruber, T., Panzeri, I., Heyne, S., Höffler, K.D., Kreiner, V., et al. (2023). Epigenetic dosage identifies two major and functionally distinct beta cell subtypes. Cell Metab. *35*, 821–836.e7. https://doi.org/10.1016/j.cmet.2023.03.008.

106. Yu, V., Yong, F., Marta, A., Khadayate, S., Osakwe, A., Bhattacharya, S., Varghese, S.S., Chabosseau, P., Tabibi, S.M., Chen, K., et al. (2024). Differential CpG methylation at Nnat in the early establishment of beta cell heterogeneity. Diabetologia *67*, 1079–1094. https://doi.org/10.1007/s00125-024-06123-6.

107. Matsuda, H., Mullapudi, S.T., Yang, Y.H.C., Masaki, H., Hesselson, D., and Stainier, D.Y.R. (2018). Whole-Organism Chemical Screening Identifies Modulators of Pancreatic beta-Cell Function. Diabetes *67*, 2268–2279. https://doi.org/10.2337/db17-1223.

108. Lawrence, M.C., Bhatt, H.S., and Easom, R.A. (2002). NFAT regulates insulin gene promoter activity in response to synergistic pathways induced by glucose and glucagon-like peptide-1. Diabetes *51*, 691–698. https://doi.org/10.2337/diabetes.51.3.691.

109. Soleimanpour, S.A., Crutchlow, M.F., Ferrari, A.M., Raum, J.C., Groff, D.N., Rankin, M.M., Liu, C., De León, D.D., Naji, A., Kushner, J.A., and Stoffers, D.A. (2010). Calcineurin signaling regulates human islet beta-cell survival. J. Biol. Chem. *285*, 40050–40059. https://doi.org/10.1074/jbc.M110.154955.

110. Kwon, G., Pappan, K.L., Marshall, C.A., Schaffer, J.E., and McDaniel, M.L. (2004). cAMP Dose-dependently prevents palmitate-induced apoptosis by both protein kinase A- and cAMP-guanine nucleotide exchange factor-dependent pathways in beta-cells. J. Biol. Chem. *279*, 8938–8945. https://doi.org/10.1074/jbc.M310330200.

111. Sonoda, N., Imamura, T., Yoshizaki, T., Babendure, J.L., Lu, J.C., and Olefsky, J.M. (2008). Beta-Arrestin-1 mediates glucagon-like peptide-1 signaling to insulin secretion in cultured pancreatic beta cells. Proc. Natl. Acad. Sci. USA *105*, 6614–6619. https://doi.org/10.1073/pnas.0710402105.

112. Furman, B., Ong, W.K., and Pyne, N.J. (2010). Cyclic AMP signaling in pancreatic islets. Adv. Exp. Med. Biol. *654*, 281–304. https://doi.org/10.1007/978-90-481-3271-3_13.

113. Tengholm, A., and Gylfe, E. (2017). cAMP signalling in insulin and glucagon secretion. Diabetes Obes. Metab. *19*, 42–53. https://doi.org/10.1111/dom.12993.

114. Dalle, S., Abderrahmani, A., and Renard, E. (2023). Pharmacological inhibitors of beta-cell dysfunction and death as therapeutics for diabetes. Front. Endocrinol. *14*, 1076343. https://doi.org/10.3389/fendo.2023.1076343.

115. Han, P., Werber, J., Surana, M., Fleischer, N., and Michaeli, T. (1999). The calcium/calmodulin-dependent phosphodiesterase PDE1C down-regulates glucose-induced insulin secretion. J. Biol. Chem. *274*, 22337–22344. https://doi.org/10.1074/jbc.274.32.22337.

116. Pratt, E.P.S., Harvey, K.E., Salyer, A.E., and Hockerman, G.H. (2019). Regulation of cAMP accumulation and activity by distinct phosphodiesterase subtypes in INS-1 cells and human pancreatic beta-cells. PLoS One *14*, e0215188. https://doi.org/10.1371/journal.pone.0215188.

117. Shibata, H., Robinson, F.W., Soderling, T.R., and Kono, T. (1991). Effects of okadaic acid on insulin-sensitive cAMP phosphodiesterase in rat adipocytes. Evidence that insulin may stimulate the enzyme by phosphorylation. J. Biol. Chem. *266*, 17948–17953.

118. Tang, X., Wang, C., Hsieh, Y., Wang, C., Wang, J., Han, Z., Cong, N., Ma, R., and Chi, F. (2019). Triptolide induces toxicity in inner ear stem cells via promoting DNA damage. Toxicol. Vitro *61*, 104597. https://doi.org/10.1016/j.tiv.2019.104597.

119. Ergin, M., Dundar, Z.D., Kilinc, I., Colak, T., Oltulu, P., and Girisgin, A.S. (2015). Alpha-Amanitin Poisoning, Nephrotoxicity and Oxidative Stress: An Experimental Mouse Model. Iran. Red Crescent Med. J. *17*, e28068. https://doi.org/10.5812/ircmj.28068.

120. Tang, D., Lahti, J.M., Grenet, J., and Kidd, V.J. (1999). Cycloheximide-induced T-cell death is mediated by a Fas-associated death domain-dependent mechanism. J. Biol. Chem. *274*, 7245–7252. https://doi.org/10.1074/jbc.274.11.7245.

121. Borowczak, J., Szczerbowski, K., Ahmadi, N., and Szylberg, Ł. (2022). CDK9 inhibitors in multiple myeloma: a review of progress and perspectives. Med. Oncol. *39*, 39. https://doi.org/10.1007/s12032-021-01636-1.

122. Su, H., Peng, C., and Liu, Y. (2024). Regulation of ferroptosis by PI3K/Akt signaling pathway: a promising therapeutic axis in cancer. Front. Cell Dev. Biol. *12*, 1372330. https://doi.org/10.3389/fcell.2024.1372330.

123. Bryanskaya, E.O., Vinokurov, A.Y., Dolgikh, A.I., Dunaev, A.V., Angelova, P.R., and Abramov, A.Y. (2024). High levels of FAD autofluorescence indicate pathology preceding cell death. Biochim. Biophys. Acta. Gen. Subj. *1868*, 130520. https://doi.org/10.1016/j.bbagen.2023.130520.

124. Oram, R.A., Sims, E.K., and Evans-Molina, C. (2019). Beta cells in type 1 diabetes: mass and function; sleeping or dead? Diabetologia *62*, 567–577. https://doi.org/10.1007/s00125-019-4822-4.

STAR★METHODS

KEY RESOURCES TABLE

REAGENT or RESOURCE	SOURCE	IDENTIFIER
Chemicals, peptides, and recombinant proteins		
Collagenase P	Sigma	Catalog #C7657
Cyclohexamide	Sigma Aldrich	C7698
Sal003	Sigma Aldrich	S4451
CCT020312	Calbiochem	324879
DHBDC	Calbiochem	5315510001
ISRIB	Sigma Aldrich	SML0843
GSK2606414/ Perk inhibitor 1	Sigma Aldrich	516535
PKRi/C16	Sigma Aldrich	I9785
Thapsigargin	Millipore	586005
Tunicamycin	Sigma Aldrich	T7765
Eeyarestatin I	Sigma Aldrich	E1286
APY 29	Sigma Aldrich	SML2381
Sunitinib	Sigma Aldrich	PZ0012
Azoramide	Sigma Aldrich	SML1560
Tacrolimus/FK506	Selleck Chem	S5003
Cylcosporin A	Selleck Chem	S2286
LY 294002	Sigma Aldrich	L9908
Wortmannin	Sigma Aldrich	W1628
Sodium butyrate	Sigma Aldrich	B5887
Trichostatin A (TSA)	Sigma Aldrich	T1952
MGCD0103/Mocetinostat	Selleck Chem	S1122
Somatostatin (SST)	Sigma Aldrich	S9129
Epinephrine	Sigma Aldrich	E4250
GLP-1 amide	R&D systems	2082
Rosiglitazone	Sigma Aldrich	R2408
Staurosporine	Sigma Aldrich	S4400
Okadaic	Sigma Aldrich	O9381
Palmitate	Sigma Aldrich	P9767
Metformin	Sigma Aldrich	PHR1084
Dexamethasone (DEX)	Sigma Aldrich	D4902
Isoxazole 9 (ISX-9)	Selleck Chem	S7914
AS1842856	Calbiochem	344355
Diazoxide	Sigma Aldrich	D9035
IBMX	Sigma Aldrich	I5879
Arginine	Sigma Aldrich	A8094
Verapamil	Sigma Aldrich	V4629
Ryanodine	Millipore	559276
5-amino-imidazole carboxamide riboside (AICAR)	Sigma Aldrich	A9978
Pramlintide	Sigma Aldrich	SML2523
Tolbutamide	Sigma Aldrich	T0891
HNMPA	Abcam	ab141566
S961	Phoenix Peptide	051–86

(*Continued on next page*)

Continued

REAGENT or RESOURCE	SOURCE	IDENTIFIER
Bortezomib	Sigma Aldrich	5043140001
MG132	Sigma Aldrich	M8699
xestospongin C	Sigma Aldrich	X2628
Actinomycin D	Sigma Aldrich	A9415
α-amanitin	Sigma Aldrich	A2263
Triptolide	Sigma Aldrich	T3652
5,6-Dichloro-1-beta-Ribo-furanosyl Benzimidazole (DRB)	Sigma Aldrich	D1916
Critical commercial assays		
Click-iT™ Plus OPP Alexa Fluor™ 647 Protein Synthesis Assay Kit	Thermofisher	Catalog #C10458
Deposited data		
Proteomics data	ProteomExchange	PXD052023
Experimental models: Organisms/strains		
Ins2^{GFP} knock-in mouse model	Wakae-Takada et al.[14]	N/A
Software and algorithms		
GraphPad Prism	Graphpad Software	N/A
ImageXpress	Molecular Devices	N/A
R	R foundation for statistical computing	N/A
STRING	STRING consortium	N/A
Cytoscape	Cytoscape Team	N/A

EXPERIMENTAL MODEL AND STUDY PARTICIPANT DETAILS

Animal husbandry

We utilized an *Ins2*^{GFP} knock-in mouse model, in which the second exon of the wild-type *Ins2* gene was partially replaced with GFP. We included both sexes in all studies performed. Animals were housed in the Modified Barrier Facility at UBC, under a protocol (#A21-0135) approved by the UBC Animal Care Committee in accordance with national and international guidelines. To maintain consistency with our prior study[15] and to keep the genotype as close to wild-type as possible, all mice in this study were *Ins2*$^{WT/GFP}$ heterozygous mice. Including the *Ins1* gene, these mice have 3 out of 4 wildtype insulin alleles. Mice used for islet isolations were between 60 and 65 weeks of age.

METHOD DETAILS

Islet isolation and dissociation

Pancreatic islets were isolated using collagenase when mice were aged 60 weeks, filtered, and hand-picked as previously described.[23] Islets were cultured overnight (37°C, 5% CO2) in RPMI1640 medium (ThermoFisher, Waltham, United States) with 11 mM glucose (Sigma), 100 units/ml penicillin, 100 μg/mL streptomycin (ThermoFisher, Waltham, United States), and 10% vol/vol fetal bovine serum (FBS; ThermoFisher, Waltham, United States). For islet dissociation, islets were washed 4 times with minimum essential medium (Corning, Corning, United States) and immersed for 5 min in 0.05% trypsin at 37°C with pipetting. Cells were then resuspended in RPMI1640 medium, plated in appropriate reservoirs or plates, and rested for 24 h (37°C, 5% CO2). Cells were incubated for 2 h in the presence of 0.05 μg/mL Hoechst 33342 (Sigma–Aldrich, St. Louis, United States) to mark nuclei and 0.5 μg/mL propidium iodide (Sigma–Aldrich, St. Louis, United States) to mark cell death. Drug/small molecules for the perturbation study were purchased from the sources indicated in Table 1 and applied immediately prior to imaging.

Fluorescence-activated cell sorting

Pancreatic islets were dispersed using 0.05% trypsin and resuspended in 1x PBS with 0.005% FBS. Dispersed islets were then filtered into 5 mL polypropylene tubes. Sorting was conducted on a Cytopeia Influx sorter (Becton Dickinson, Franklin Lakes, USA) at the Life Sciences Institute FLOW core facility. Cells were excited with a 488 nm laser (530/40 emission) and a 561 nm laser (610/20 emission).

Live cell imaging and analysis

For 3D live imaging, intact mouse islets were incubated overnight in culture media (RPMI1640 medium with 11 mM glucose, 100 units/ml penicillin, 100 μg/mL streptomycin, and 10% vol/vol FBS) with Hoechst 33342 (0.05 μg/mL) and propidium iodide

(0.5 μg/mL). After 24 h, cells were transferred into 2 well or 8 well μ-Slides (Ibidi) with fresh culture media. Images were then acquired using a LEICA THUNDER Imager Live Cell & 3D assay microscope at 25× water objective (numerical aperture 0.95). Analysis of 3D live cell imaging experiments was done using Imaris Microscopy Image Analysis software with the FIJI Labkit module and custom R scripts. Image processing, including smoothing and background subtraction, was performed using Imaris. Labkit facilitated image labeling and pixel classification for the identification of GFP fluorescence in individual β cells. Nearest neighbor analysis was done using Imaris Python XTensions. Distance-to-core analysis was conducted on Imaris, using a reference frame positioned at the islet's center to measure the distance of each cell from the origin reference frame. Plots were generated for visualization using Graphpad Prism v10 or custom R scripts.

To investigate the effects of small molecules on GFP fluorescence, we cultured dispersed islet cells from *Ins2*^{GFP} mice on 384-well glass bottom plates (PerkinElmer, Waltham, United States) and performed live cell imaging using an ImageXpress^{Micro} environmentally controlled, robotic system (Molecular Devices, San Jose, United States) which employed a 300 W Xenon lamp as previously described.[1] Cells were stained with Hoechst 33342 and propidium iodide as described above. Images were acquired at 10× air objective, numerical aperture 0.3, at 30-min intervals up to 96 h, with cells being exposed to 359 nm light for 110 ms, 491 nm light for 15 ms, 561 nm for 75 ms. Analysis of live cell imaging experiments on *Ins2*^{GFP} cells was done using MetaXpress analysis software and custom R scripts. Tracking of GFP fluorescence in individual cells was performed as previously described.[15] The *Ins2*(GFP)^{HIGH} and *Ins2*(GFP)^{LOW} subpopulations were identified using model-based clustering.[15]

Protein synthesis assay

One day after isolation, dispersed islets were seeded into an optical 96-well plate (PerkinElmer, Waltham, United States) at a density of approximately 16,000 cells per well in culture media (RPMI1640 medium with 11 mM glucose, 100 units/ml penicillin, 100 μg/mL streptomycin, and 10% vol/vol FBS). Treatments were applied 3 h after seeding. After 24 h of incubation, fresh culture media was applied, then supplemented with 20 μM OPP (Invitrogen, Waltham, United States). The assay was performed according to instructions provided by the manufacturer. Cells were imaged at 10x, numerical aperture 0.3, with an ImageXpress^{Micro} high-content imager and analyzed with MetaXpress to quantify the integrated staining intensity of OPP-Alexa Fluor 594 in cells identified by NuclearMask Blue Stain.

Mass spectrometry/proteomics

For proteomics sample preparation, between 2,000 and 10,000 cells were diluted with ultrapure water, and then lysed by adding cold trifluoroethanol (TFE) (final 50% TFE) to the suspension. Samples were then chilled on ice for 10 min, vortexed for 1 min and further sonicated for 5–10 min in an ice bath. Tris (pH 8–8.5) was added to adjust the pH and concentration to final 100 mM Tris at pH 8–8.5. Total protein mass was estimated to be 0.3 ng/cell. Samples were reduced with tris(2-carboxyethyl)phosphine (1 μg TCEP: 50 μg protein) incubated for 20 min at room temperature, then alkalized with chloroacetamide (5 μg CAA:50 μg protein) incubated at 95°C for 10 min. Then samples were diluted with 50mM Ammonium bicarbonate (final TFE <10%). Proteins were digested with LysC/Trypsin (1 μg LysC/Trypsin: 50 μg protein) for 2 h at 37°C, followed by digestion with trypsin (1 μg trypsin: 50 μg protein) and incubated overnight at 37°C. Samples were further digested with trypsin (1 μg trypsin: 125 μg protein) for 5 h at 37°C. Digestion was stopped by acidification. Samples were desalted with 6 mm depth of C18; briefly, STAGE (stop and go extraction) tips were conditioned with 100% methanol, equilibrated with 0.2% TFA, loaded with samples, then washed with 0.2% TFA, and finally eluted with 80 μL *2 of 40% ACN, 0.1% formic acid. Eluate was dried in vacuum then kept in −20°C. Before instrumental analysis, samples were reconstituted in in 0.5% acetonitrile, 0.1% formic acid and concentration was measured using NanoDrop One (ThermoFisher, Waltham, USA) with the A205 Scopes method (absorbance at 205 nm, baseline correction at 340 nm).

For liquid chromatography steps, 75 ng of peptides were injected and separated on-line using NanoElute UHPLC system (Bruker Daltonics Billerica, United States) with Aurora Series Gen2 (CSI) analytical column, (25 cm × 75 μm 1.6μm FSC (fuse silica core) C18, with Gen2 nanoZero and CSI (captive spray interface) fitting; Ion Opticks, Parkville, Australia) heated to 50°C and coupled to timsTOF Pro (Bruker Daltonics, Billerica, USA). A standard 30 min gradient was run from 2% buffer B to 12% buffer B over 15 min, then to 33% B from 15 to 30 min, then to 95% B over 0.5 min, and held at 95% B for 7.72 min. Before each run, the analytical column was conditioned with 4 column volumes of buffer A. Where buffer A consisted of 0.1% aqueous formic acid and 0.5% acetonitrile in water, and buffer B consisted of 0.1% formic acid in 99.4% acetonitrile. The NanoElute thermostat temperature was set at 7°C. The analysis was performed at 0.3 μL/min flow rate.

For mass spectrometry steps, the Trapped Ion Mobility – Time of Flight Mass Spectrometer (TimsTOF Pro; Bruker Daltonics, Billerica, USA) was set to Parallel Accumulation-Serial Fragmentation (PASEF) scan mode for DIA acquisition scanning 100–1700 m/z. The capillary voltage was set to 1800V, drying gas to 3 L/min, and drying temperature to 180°C. The MS1 scan was followed by 17 consecutive PASEF ramps containing 22 non-overlapping 35 m/z isolation windows, covering the m/z range 319.5–1089.5 (more information in DIA windows). As for TIMS setting, ion mobility range (1/k0) was set to 0.70–1.35 V s/cm^2, 100 ms ramp time and accumulation time (100% duty cycle), and ramp rate of 9.42 Hz; this resulted in 1.91s of total cycle time. The collision energy was ramped linearly as a function of mobility from 27 eV at 1/k0 = 0.7 V s/cm^2 to 55 eV at 1/k0 = 1.35 V s/cm^2. Mass accuracy: error of mass measurement is typically within 3 ppm and is not allowed to exceed 7 ppm. TimsTOF Pro was run with timsControl v. 4.1.12 (Bruker, Billerica, USA). LC and MS were controlled with HyStar 6.0 (6.2.1.13, Bruker, Billerica, United States). For the final search and quantification of the results, acquired diaPASEF data were then searched using DIA-NN (v. 1.8.1) to obtain DIA quantification, with the

spectral library generated from the canonical proteome for *Mus Musculus* from UniProt. Quantification mode was set to "Any LC (high precision) and a two-pass search was completed. All other settings were left default. Mice with a GFP protein ratio of less than 3 when comparing their respective *Ins2*(GFP)^{HIGH} and *Ins2*(GFP)^{LOW} samples were excluded. Proteomic data are available on ProteomExchange (number PXD052023).

QUANTIFICATION AND STATISTICAL ANALYSIS

Statistics and data visualization

Statistics and data representation for nearest neighbor analyses, distance to core analyses, and OPP translation assays, were conducted using GraphPad Prism v10 (GraphPad Software, San Diego, USA). Statistics and data representation for live cell imaging experiments employed custom R scripts. Student's t test and one-way ANOVAs were used for parametric data as indicated in figure legends. For all statistical analyses, differences were considered significant if the p value was less than 0.05 and were abbreviated with an asterisk (*). Error bars were presented as ± standard error of the mean (SEM).

For proteomics analyses, proteins that were present in less than 80% of samples were removed from analysis. Significantly differential proteins were defined with a threshold of p value <0.05 and a fold-change of more than 20%, and graphs were generated using custom R scripts. For STRING and Cytoscape analyses, significantly differentially abundant proteins were entered into the STRING website, where nodes and networks were generated. For STRING settings, only 'Experiments' and 'Databases' interactions were included, with medium confidence interaction scores. STRING networks and protein expression data were then imported into Cytoscape and reordered according to their cellular location. Background images were generated with Biorender.

For STRING and Cytoscape analyses in our small molecule screen, the primary binding proteins for small molecules were determined using online literature search. Proteins were then entered into STRING, where nodes and networks were rendered. For settings on STRING, all interactions were included, with medium confidence interaction scores. STRING networks, GFP fluorescence, cell death, and cell state transition data were then imported and finalized in Cytoscape. Background graphs were generated using Biorender.